nature cell biology

ARTICLES

# A 14-3-3γ dimer-based scaffold bridges CtBP1-S/BARS to PI(4)KIIIβ to regulate post-Golgi carrier formation

Carmen Valente[1,2,3], Gabriele Turacchio[1,3], Stefania Mariggiò[1,3], Alessandro Pagliuso[1,2,3], Renato Gaibisso[3], Giuseppe Di Tullio[3], Michele Santoro[2,3], Fabio Formiggini[4,5], Stefania Spanò[3,7], Daniele Piccini[6], Roman S. Polishchuk[2,3], Antonino Colanzi[1,3], Alberto Luini[1,2,3,8] and Daniela Corda[1,3,8]

**Large pleiomorphic carriers leave the Golgi complex for the plasma membrane by *en bloc* extrusion of specialized tubular domains, which then undergo fission. Several components of the underlying molecular machinery have been identified, including those involved in the budding/initiation of tubular carrier precursors (for example, the phosphoinositide kinase PI(4)KIIIβ, the GTPase ARF, and FAPP2), and in the fission of these precursors (for example, PKD, CtBP1-S/BARS). However, how these proteins interact to bring about carrier formation is poorly understood. Here, we describe a protein complex that mediates carrier formation and contains budding and fission molecules, as well as other molecules, such as the adaptor protein 14-3-3γ. Specifically, we show that 14-3-3γ dimers bridge CtBP1-S/BARS with PI(4)KIIIβ, and that the resulting complex is stabilized by phosphorylation by PKD and PAK. Disrupting the association of these proteins inhibits the fission of elongating carrier precursors, indicating that this complex couples the carrier budding and fission processes.**

Intracellular membrane trafficking relies on membrane-bound carriers that travel between donor and acceptor compartments. These carriers belong to two main classes: small round vesicles that form by virtue of protein coats (for example, coat protein complex I (COPI), coat protein complex II (COPII) and clathrin), and much larger pleiomorphic containers devoid of visible coats[1–3]. Among the latter, the best studied are those involved in transport from the Golgi complex to the basolateral plasma membrane (basolateral post-Golgi carriers, or PGCs). The formation of PGCs has been extensively characterized with respect to morphology and dynamics, and has been shown to occur in two stages: *en bloc* extrusion of elongated tubular precursors from specialized trans-Golgi network (TGN) export domains[3], and fission of these precursors into free-moving carriers[1,4]. The molecular mechanisms of PGC formation, however, are not completely understood[5,6].

So far, the molecular sequence involved in the formation of PGCs has been shown to comprise (1) ADP-ribosylation factor (ARF)-induced recruitment to the TGN and activation (enhanced by neuronal calcium sensor-1 (NCS-1); ref. 7) of phosphatidylinositol 4-kinase IIIβ(PI(4)KIIIβ), with production of phosphatidylinositol 4-phosphate (PtdIns4P; refs 8–10), (2) PtdIns4P- (and ARF-) induced recruitment of the glycolipid-transfer protein FAPP2 (also known as PLEKHA8; proposed to facilitate membrane bending[9,11,12]) and (3) docking of the forming tubular precursors to specific kinesin motors that pull them out of the Golgi along microtubules[1]. These proteins (presumably with several uncharacterized factors) are thus involved in initiation and protrusion of tubular precursors.

Another set of proteins is instead involved in the fission of these precursors. These include: protein kinase D (PKD), with its activators and modulators[13–15]; myosin II and Rab6 (ref. 16); and CtBP1-S/BARS (for brevity, BARS; ref. 17), a dual-function protein with key roles in the nucleus and the cytosol[18,19], where it is required for various membrane fission events[19,20].

These components must act in concert to form PGCs. It is thus essential to understand how they assemble and disassemble throughout the carrier-extrusion and fission processes. Here, using BARS as bait, we have identified a protein complex that includes BARS, ARF,

[1]Institute of Protein Biochemistry, National Research Council, Via Pietro Castellino 111, 80131 Naples, Italy. [2]Telethon Institute of Genetics and Medicine, Via Pietro Castellino 111, 80131 Naples, Italy. [3]Department of Cell Biology and Oncology, Consorzio Mario Negri Sud, Via Nazionale, 66030 Santa Maria Imbaro, Chieti, Italy. [4]Fondazione Istituto Italiano di Tecnologia IIT@CRIB, Center for Advanced Biomaterials for Health Care, Largo Barsanti e Matteucci 53, 80125 Naples, Italy. [5]CEINGE Biotecnologie Avanzate, via Gaetano Salvatore 482, 80145 Naples, Italy. [6]Fondazione Istituto FIRC di Oncologia Molecolare (IFOM), IFOM-IEO, Via Adamello 16, 20139 Milan, Italy. [7]Present address: Section of Microbial Pathogenesis, Yale University School of Medicine, Boyer Center for Molecular Medicine, New Haven, Connecticut 06536, USA.
[8]Correspondence should be addressed to A.L. or D.C. (e-mail: alberto.luini@cnr.it or d.corda@ibp.cnr.it)

Received 12 August 2011; accepted 17 January 2012; published online 26 February 2012; DOI: 10.1038/ncb2445

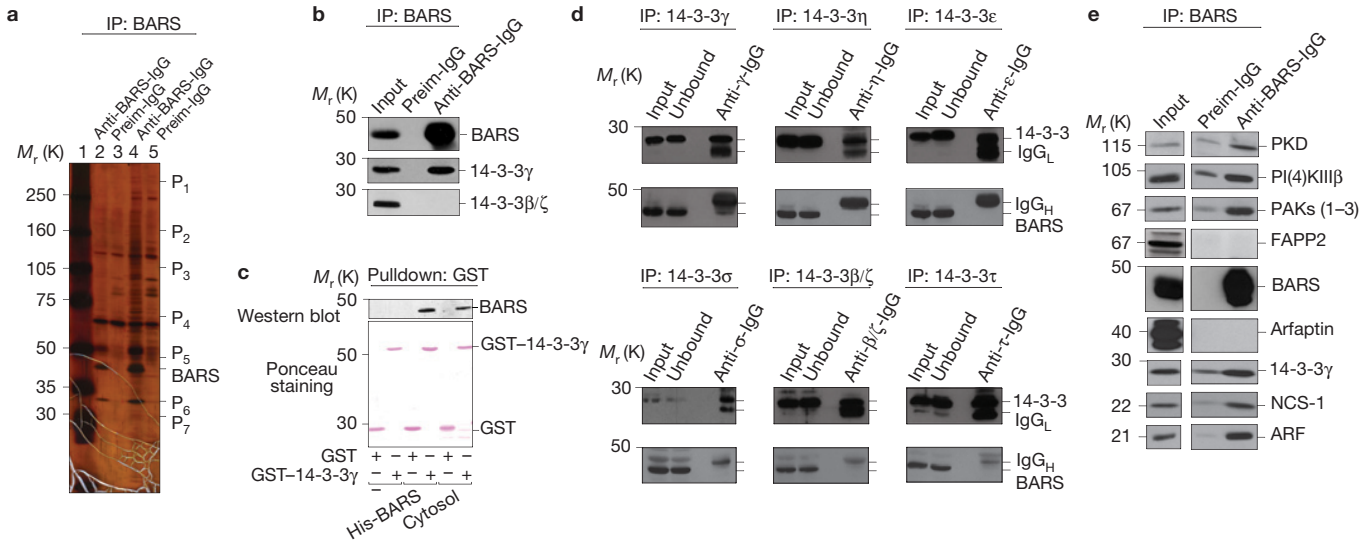


**Figure 1** BARS interacts with 14-3-3γ and several proteins involved in PGC formation. (**a**,**b**) BARS immunoprecipitation (IP: BARS) of rat-brain cytosol with preimmune-IgG (Preim-IgG) or anti-BARS-IgG matrices. (**a**) The proteins bound to preim-IgG and to anti-BARS-IgG (as indicated) were eluted with glycine (lanes 2, 3, second eluted fractions; lanes 4, 5, third eluted fractions), separated by SDS–PAGE, and revealed by silver staining. $P_{1-7}$ indicate specific BARS-interacting proteins identified by mass spectrometry. $P_7$ is 14-3-3γ. (**b**) Representative western blotting (antibodies as indicated) of total cytosol (input) and immunoprecipitated proteins. 14-3-3γ, and not 14-3-3β/ζ, co-precipitates with BARS. (**c**) GST pulldown of equimolar amounts of recombinant GST and GST–14-3-3γ, for buffer alone (−), recombinant His–BARS and rat-brain cytosol. Elution with reduced glutathione, followed by western blotting with a monoclonal anti-BARS antibody (top), with pulled-down proteins revealed by Ponceau-S staining (bottom). (**d**) Immunoprecipitation (IP) of rat-brain cytosol with specific antibodies against 14-3-3 isoforms (as indicated). Representative western blotting with isoform-specific 14-3-3 antibodies and an anti-BARS antibody, of total cytosol (input), unbound protein and immunoprecipitated protein (as indicated). $IgG_L$, IgG light chain; $IgG_H$, IgG heavy chain. BARS is only detected in association with 14-3-3γ. (**e**) BARS immunoprecipitation (IP: BARS) of COS7 cell lysates with preim-IgG or anti-BARS-IgG matrices. Representative western blotting (antibodies as indicated) of total lysate (input) and immunoprecipitated proteins. Molecular-weight standards ($M_r$ (K)) are indicated on the left of each panel. Uncropped images of blots are shown in Supplementary Fig. S9.1.

PI(4)KIIIβ, NCS-1, the kinases PKD and p21-activated kinase (PAK), and some other components. One of these others is the γ isoform of a protein family, the 14-3-3s, that is involved in many functions, including the assembly of molecular complexes[21]. Moreover, some 14-3-3s can bind PI(4)KIIIβ in mammals[22] and in yeast[23]. We find that 14-3-3γ dimers (14-3-3γ(2)) act at the Golgi complex as a scaffold in the assembly of a PI(4)KIIIβ–14-3-3γ(2)–BARS complex. This core complex is associated with ARF and NCS-1, and is stabilized by phosphorylation by the kinases PKD and PAK. If formation of the PI(4)KIIIβ–14-3-3γ(2)–BARS core is inhibited, tubular precursors can still form, but their fission no longer occurs, indicating that the complex acts to coordinate carrier budding–tubulation with tubule fission.

## RESULTS

### BARS interacts with 14-3-3γ and with several proteins involved in PGC formation

We first used rat-brain cytosol and a specific anti-BARS antibody[24] for co-precipitation of BARS interactors, followed by their identification by mass spectrometry. One of the interactors thus isolated was 14-3-3γ (Fig. 1a). We confirmed this interaction by western blotting (Fig. 1b), and showed that it is (1) direct, using purified recombinant His–BARS and glutathione *S*-transferase (GST)–14-3-3γ in *in vitro* binding assays (Fig. 1c), and (2) isoform specific, as BARS co-precipitates with the γ, and not with the η, ε, σ, β, ζ and τ, 14-3-3 isoforms (Fig. 1d).

Next, we used lysates from COS7 cells as a source of interactors, as these cells are a well-characterized system with respect to the BARS membrane-fission activity[17]. Here, we screened a large number of proteins by western blotting, with a focus on those proposed to be involved in the formation of PGCs (see above). We found that, in addition to 14-3-3γ, PI(4)KIIIβ and its activators ARF1 and NCS-1, as well as the fission-inducing kinase PKD (refs 7,10,25,26), the p21-activated kinases (group I PAKs; PAKs 1–3; ref. 27) co-precipitated with BARS (Fig. 1e); whereas further Golgi proteins, including FAPP2, arfaptin (Fig. 1e), dynamin and phosphatidylinositol-transfer proteins (not shown), did not co-precipitate with BARS. These results suggest that BARS is part of a protein complex that is involved in carrier formation and includes 14-3-3γ.

### 14-3-3γ is required for BARS-dependent fission of PGCs

To examine the role of 14-3-3γ in carrier formation, we depleted COS7 cells of 14-3-3γ using specific short interfering (si)RNAs that did not affect the levels of other 14-3-3 isoforms (Fig. 2a). These depleted cells were then tested in a Golgi-to-plasma-membrane transport assay[17] based on a temperature-sensitive variant of the viral protein VSVG (ts045-VSVG; for brevity, VSVG; ref. 28). This VSVG variant cannot fold at 40 °C and is retained in the endoplasmic reticulum; but it exits the endoplasmic reticulum at lower temperatures. VSVG was first accumulated in the endoplasmic reticulum at 40 °C, and then temperature was shifted to 20 °C, a temperature at which cargo proteins exit the endoplasmic reticulum and reach, but cannot exit, the TGN (ref. 29). The temperature was finally shifted to 32 °C, and transport from the TGN to the plasma membrane was monitored (Fig. 2b,c). Depletion of 14-3-3γ had no effect on transport to the TGN, but it inhibited transport from the TGN to the plasma membrane (Fig. 2b,c).

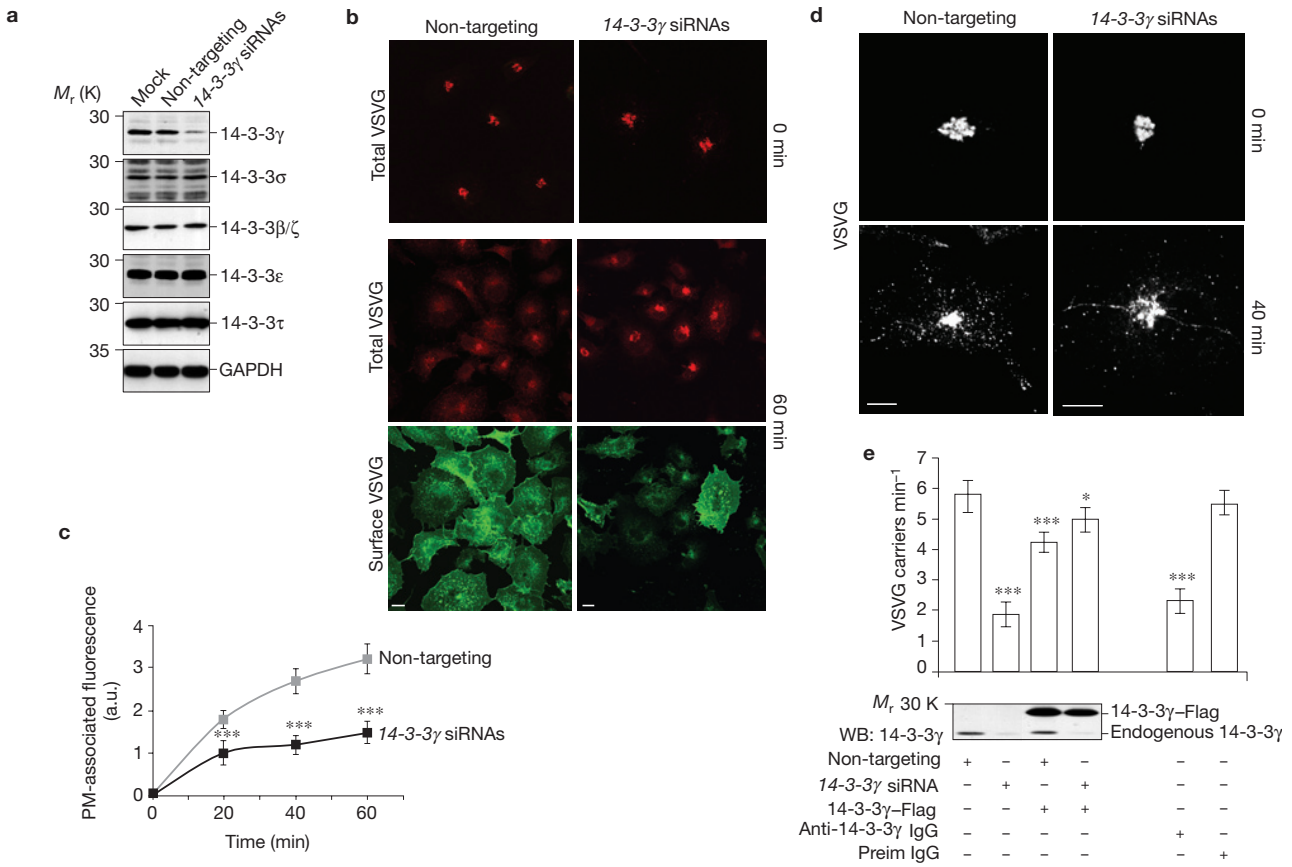


**Figure 2** 14-3-3γ depletion reduces VSVG-positive PGC formation. (**a**) COS7 cells were left untreated (Mock) or treated with non-targeting or with *14-3-3γ* siRNAs, and the efficiency of interference was monitored by western blotting of cell lysates using isoform-specific 14-3-3 antibodies. Glyceraldehyde 3-phosphate dehydrogenase (GAPDH) levels are shown for overall protein levels. *14-3-3γ* siRNA treatment has no effect on expression of the other 14-3-3 isoforms. (**b**–**e**) COS7 cells transfected with non-targeting or *14-3-3γ* siRNAs (**b**–**d**, pool; **e**, duplex 2) (except for IgG-microinjected cells), vesicular stomatitis virus (VSV) infected and subjected to the TGN-exit assay. (**b**) Representative confocal microscopy images of cells fixed after the 20 °C block (0 min) or 60 min after 32 °C temperature-block release. Total VSVG: stained after permeabilization (red, P5D4 anti-VSVG antibody). Surface VSVG: stained without permeabilization (green, lumenal domain anti-VSVG antibody). (**c**) Quantification of time course in **b**, with plasma-membrane (PM)-associated VSVG as ratio of plasma membrane:total VSVG. (**d**) Representative confocal microscopy images of cells subjected to TGN-exit assay with 0.5% tannic acid. The cells were fixed following the 20 °C block (0 min) or 40 min after the shift to 32 °C, and stained for VSVG-positive PGCs. PGC tubular precursors are generally seen in about 30% of fixed cells owing to the dynamic nature of the tubular elements and their low resistance to the fixatives[31]. (**e**) Quantification of VSVG-containing PGCs in **d**. Cells were also transfected before VSV infection and TGN-exit assay without or with 14-3-3γ–Flag encoding silent mutations. Far right: following VSV infection and during TGN-exit assay (after 1 h at 20 °C), the cells were microinjected with preim-IgG and anti-14-3-3γ-IgG (1 mg ml$^{-1}$ commercial anti-14-3-3γ polyclonal antibody) and incubated for a further 3 h at 20 °C. All cells were fixed 30 min after the shift to 32 °C, and PGCs quantified. Panel: efficiency of interference and overexpression by western blotting (WB; monoclonal anti-14-3-3γ antibody). Data in **c**,**e** are means ± s.d. of three independent experiments. $^{*}P < 0.05$, $^{***}P < 0.005$ (Student's *t*-test). Scale bars, 10 μm. Uncropped images of blots are shown in Supplementary Fig. S9.1.

This inhibition might be due to a reduction in PGC formation or in PGC fusion with the plasma membrane[3]. To distinguish between these possibilities, we treated cells with tannic acid, which prevents carrier fusion with the plasma membrane[30], resulting in accumulation of carriers in the cell periphery. This accumulation was inhibited by depletion of 14-3-3γ and by microinjection of an anti-14-3-3γ antibody (Fig. 2d,e). This effect was specific because (1) it was prevented by transfection with an siRNA-resistant version of 14-3-3γ (Fig. 2e) and (2) it was not induced by depletion of other 14-3-3 isoforms (Fig. 3a,b and Supplementary Fig. S1). Thus, 14-3-3γ is required for carrier formation. This, in turn, might be due to a role for 14-3-3γ in carrier budding or in carrier fission from the Golgi. We sought to distinguish between these possibilities by examining the dynamics of carrier formation in live cells (Golgi tubules are often fragmented by fixatives)[31] (see legends to Fig. 2d and Supplementary Movies S1 and S2). In control cells, tubular carriers (1–8 μm long) formed from the Golgi and then detached and moved to the plasma membrane, as previously described[3] (Supplementary Movie S1). Instead, in 14-3-3γ-depleted cells, most tubular carriers did not detach, and continued to elongate out from, and then retract back into, the Golgi (Supplementary Movie S2). These tubules ranged from 5 μm to 30 μm in length (Supplementary Movie S2), and elongated at a rate consistent with microtubule-based motility[3]. Altogether, these observations indicate that 14-3-3γ is required for fission of tubular carrier precursors.

We next examined whether BARS and 14-3-3γ are involved in the same fission event by exploiting our previous observation that acute enhancement of intracellular BARS results in rapid formation of PGCs (ref. 17). VSVG–GFP (green fluorescent protein) was accumulated in the TGN at 20 °C, to monitor PGC formation in control and

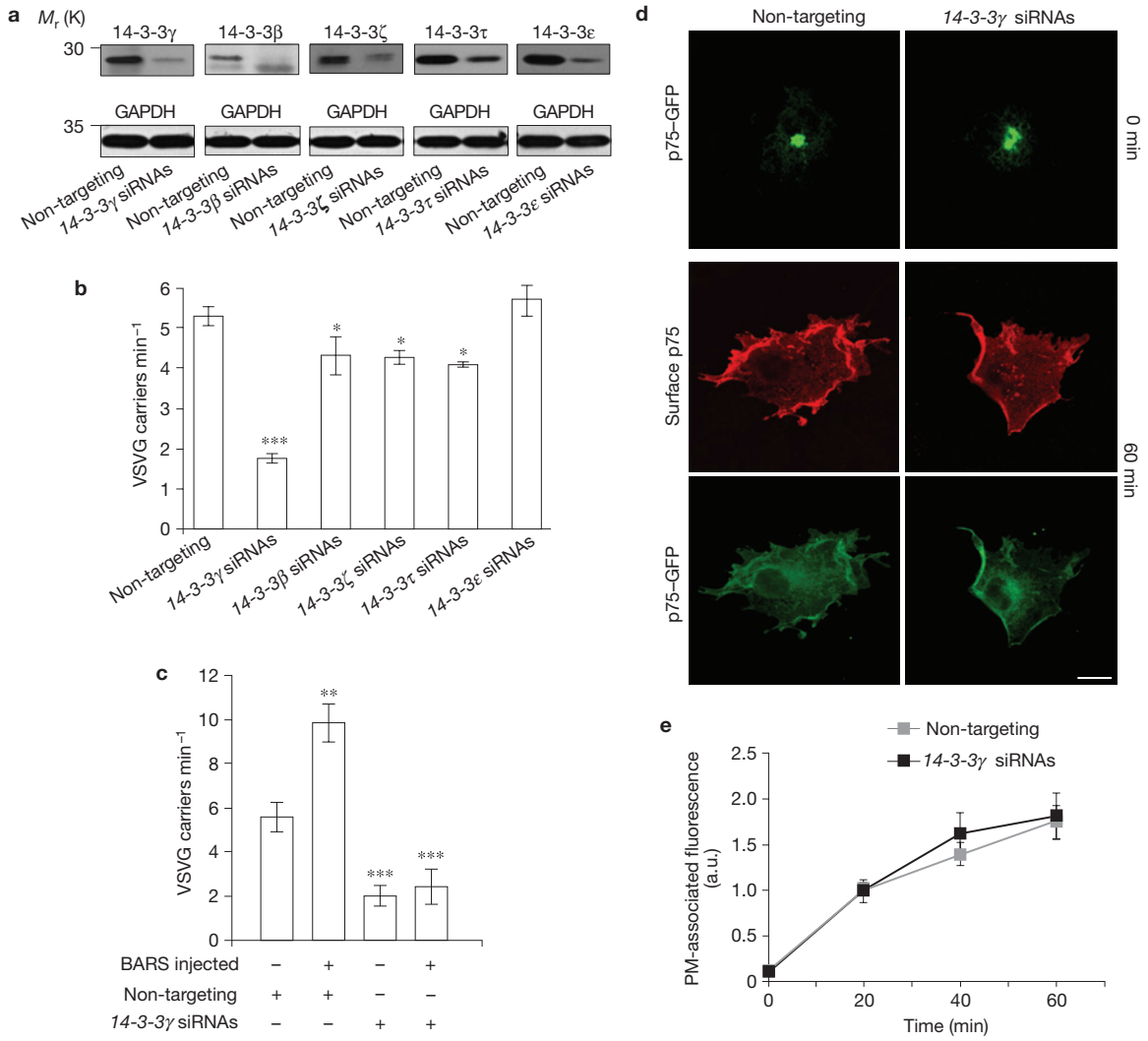


**Figure 3** 14-3-3γ is required for BARS-dependent fission of post-Golgi carriers. (**a**–**e**) COS7 cells were transfected with non-targeting or *14-3-3γ*, *β*, *ζ*, *τ* and *ε* siRNAs (as indicated), and infected with VSV (**b**,**c**) or transfected with a plasmid encoding p75–GFP (**d**,**e**), and subjected to the TGN-exit assay with (**b**,**c**) or without (**d**,**e**) 0.5% tannic acid. Although COS7 cells are not polarized, they direct cargoes with either basolateral or apical sorting signals into distinct BARS-dependent and BARS-independent post-Golgi transport routes, respectively[17]. (**a**) Efficiency of interference by western blotting (with isoform-specific anti-14-3-3 and anti-GAPDH antibodies). (**b**,**c**) Quantification of VSVG-positive PGCs in 14-3-3-isoform-specific (**b**) or 14-3-3γ-specific (**c**) interfered cells. 14-3-3γ depletion causes strong inhibition of PGC formation (with minor decreases in 14-3-3β-, *ζ*- and *τ*-depleted cells and a minor increase in 14-3-3ε-depleted cells, perhaps due to non-specific effects). In **c**, during the TGN-exit assay (after 1 h at 20 °C), the cells were microinjected with recombinant GST–BARS (2–3 mg ml$^{-1}$; BARS injected), and incubated for a further 2 h at 20 °C. All cells were fixed 30 min after shift to 32 °C. (**d**) Representative confocal microscopy images of cells after 48 h interference and transfection with a plasmid encoding p75–GFP, and TGN-exit assay for p75, with fixing at the end of the 20 °C block (0 min) or 60 min after shift to 37 °C. Without permeabilization, the antibody against the p75 lumenal domain shows surface staining of p75 (red). Scale bar, 10 μm. (**e**) Quantification of time course in **d**, for arrival of p75 at the plasma membrane (PM), measured as ratio of plasma-membrane-localized:total p75–GFP. Data in **b**,**c**,**e** are means ± s.d. of three independent experiments. $^{*}P < 0.05$, $^{**}P < 0.01$, $^{***}P < 0.005$ (Student's *t*-test). Uncropped images of blots are shown in Supplementary Fig. S9.1.

14-3-3γ-depleted COS7 cells, and then cells were microinjected with recombinant BARS. In control cells, this treatment triggered the expected increase in PGC formation (ref. 17 and see Fig. 3c), whereas in 14-3-3γ-knockdown cells it had no effect (Fig. 3c), and long VSVG-containing tubules continued to form without detaching, consistent with impaired fission (not shown). Analogous results were obtained by inducing rapid and intense BARS overexpression. This treatment increased the PGCs in control, but not in 14-3-3γ-depleted, cells (Supplementary Movie S3). These data indicate that BARS requires 14-3-3γ to induce fission.

Finally here, we noted that BARS controls Golgi export of basolaterally directed cargo proteins, but not of apically directed ones (such as p75; ref. 32), which, instead, require dynamin[17]. Therefore, if 14-3-3γ cooperates selectively with BARS, its role should be restricted to basolateral transport. To verify this hypothesis, we examined export of p75–GFP from the Golgi. No differences in p75 transport were detected between control and 14-3-3γ-depleted cells (Fig. 3d,e). In conclusion, 14-3-3γ is selectively required for the fission-inducing effects of BARS on tubular basolateral PGC precursors. An apparent discrepancy here is that 14-3-3γ-knockout mice do not show any overt

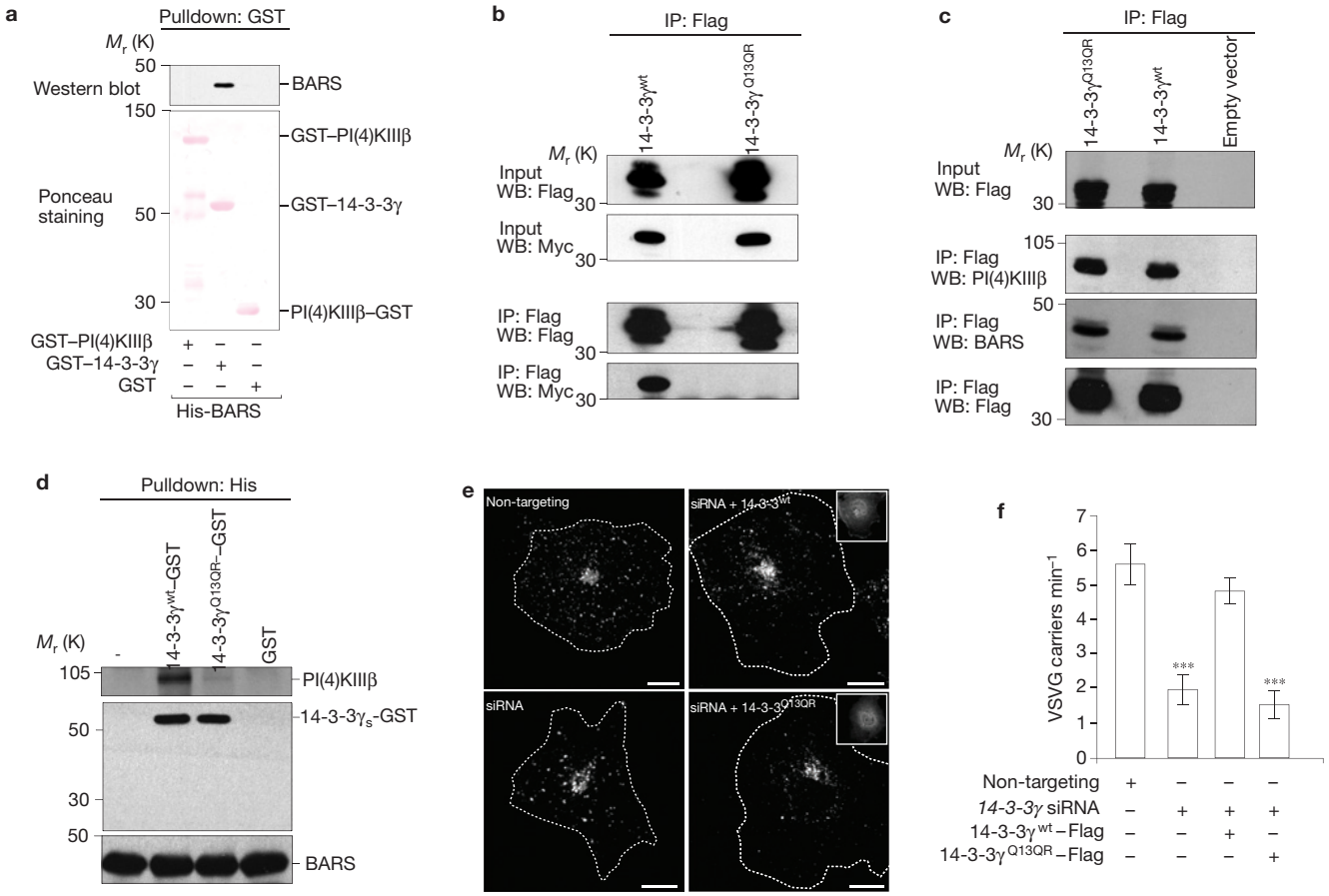


**Figure 4** The 14-3-3γ dimer bridges BARS and PI(4)KIIIβ and has a role in VSVG-positive PGC formation. (**a**) GST pulldown of equimolar amounts of GST, GST–PI(4)KIIIβ and GST–14-3-3γ, for His–BARS, with eluted proteins analysed by western blotting (top, anti-BARS monoclonal antibody). GST fusion proteins revealed by Ponceau-S staining (bottom). (**b**) Immunoprecipitation (IP) for 14-3-3γ dimerization residues with an anti-Flag antibody, of lysate from COS7 cells co-transfected with plasmids encoding Flag-tagged and Myc-tagged 14-3-3$\gamma^{wt}$ or 14-3-3$\gamma^{Q13QR}$. Analysis by western blotting (WB) with anti-Flag or anti-Myc antibodies (as indicated) of total lysate (input) and Flag-immunoprecipitated proteins. (**c**) Immunoprecipitation (IP) with anti-Flag antibody, of calyculin-A-treated lysate from COS7 cells transfected with 14-3-3$\gamma^{Q13QR}$–Flag, 14-3-3$\gamma^{wt}$–Flag or empty vector. Analysis by western blotting (WB) with anti-Flag antibody, of total lysate (top; input), and with anti-Flag, anti-PI(4)KIIIβ and polyclonal anti-BARS antibodies for Flag-immunoprecipitated proteins (bottom). (**d**) Histidine pulldown for His–BARS beads, of buffer alone (–) or equimolar GST, 14-3-3$\gamma^{wt}$–GST or 14-3-3$\gamma^{Q13QR}$–GST. Beads were incubated with rat-brain cytosol, with eluted proteins analysed by western blotting using anti-PI(4)KIIIβ, polyclonal anti-GST or monoclonal anti-BARS antibodies (as indicated). (**e**) Representative images of COS7 cells transfected with non-targeting or a 14-3-3γ siRNA (duplex 2), and with 14-3-3$\gamma^{wt}$–Flag or 14-3-3$\gamma^{Q13QR}$–Flag mutant encoding silent mutations and subjected to VSV infection and TGN-exit assay with 0.5% tannic acid. Cells were fixed 30 min after shift to 32 °C and processed for immunofluorescence with the anti-Flag antibody and with the p5D4 anti-VSVG antibody to monitor formation of VSVG-containing PGCs. Insets: 14-3-3$\gamma^{wt}$–Flag- or 14-3-3$\gamma^{Q13QR}$–Flag-expressing cells, as indicated. Scale bars, 10 μm. Note that the localization of expressed 14-3-3γ–Flag is not restricted to the Golgi, probably because the 14-3-3γ Golgi binding sites are saturated under this condition. (**f**) Quantification of VSVG-containing PGCs in COS7 cells treated as in **e**. Data are means ± s.d. of three independent experiments. $^{***}P < 0.005$ (Student's *t*-test). Uncropped images of blots are shown in Supplementary Fig. S9.2.

phenotype[33]. However, discrepancies of this kind are common, and can be attributed to redundancy among the mechanisms involved, and to adaptive processes that take place in the embryo[17].

## A 14-3-3γ dimer bridges BARS and PI(4)KIIIβ and is required for post-Golgi basolateral carrier formation

As noted, BARS co-precipitates with several proteins involved in PGC formation (Fig. 1e). We asked whether, and how, these proteins might form a complex. We first examined the interaction between BARS and PI(4)KIIIβ. As shown above, BARS co-precipitates with PI(4)KIIIβ from cell lysates (Fig. 1e); however, purified recombinant BARS and PI(4)KIIIβ mixed *in vitro* did not associate (Fig. 4a). We reasoned that BARS might be bridged to PI(4)KIIIβ through a 14-3-3γ dimer. This was indicated by the following observations: (1) BARS binds 14-3-3γ directly (Figs 1c and 4a); (2) other 14-3-3 proteins bind PI(4)KIIIβ (ref. 22); (3) 14-3-3γ is a dimer[34] with binding sites at each of its two poles[35] and (4) other 14-3-3 isoforms act as bridges in protein complexes[36–38]. This bridging model predicts that 14-3-3γ binds directly with both BARS (as shown above) and PI(4)KIIIβ. We thus examined its interaction with PI(4)KIIIβ and found that (1) recombinant 14-3-3γ interacts with PI(4)KIIIβ from brain cytosol or from Golgi membranes (Supplementary Fig. S2a) and (2) recombinant 14-3-3γ binds to recombinant PI(4)KIIIβ *in vitro* (Supplementary Fig. S2b). Thus, both BARS and PI(4)KIIIβ can bind 14-3-3γ directly.

Next, we used different approaches to determine whether BARS and PI(4)KIIIβ can bind to the same 14-3-3γ dimer. First, we passed cell lysates through two sequential ion-exchange fast protein liquid chromatography columns (MonoQ and MonoS), as described earlier for other 14-3-3-bridged proteins[36]. BARS, 14-3-3γ and PI(4)KIIIβ showed relatively broad elution profiles from the MonoQ column. The 'overlap' fractions were pooled and run through the MonoS column. Here, the three proteins showed similar elution profiles. Moreover, and importantly, they all co-immunoprecipitated efficiently from the MonoS eluate (ref. 36 and Supplementary Fig. S2c), indicating that they form a stable complex. Second, to further test the bridging role of 14-3-3γ, we used an *in vitro* pulldown assay[38] based on a 14-3-3γ mutant designed to be monomeric (Fig. 4 caption) and at the same time to maintain binding to BARS or PI(4)KIIIβ (Fig. 4b–d). We generated bead-immobilized His–BARS bound to wild-type (dimeric) or mutated (monomeric) GST–14-3-3γ, and then incubated these complexes with brain cytosol. As expected, the BARS complex with dimeric 14-3-3γ efficiently bound PI(4)KIIIβ. Instead, the BARS complex with monomeric 14-3-3γ was very inefficient in binding PI(4)KIIIβ (Fig. 4d). Thus, BARS and PI(4)KIIIβ can be bridged by a 14-3-3γ dimer. The mechanism by which a 14-3-3 dimer associates with two different proteins, rather than binding twice to the same molecule, remains unclear; however, examples of this kind have been reported: for instance, 14-3-3s bridge Raf and Bcr (ref. 36), Raf and A20 (ref. 37) and Raf and protein kinase C (PKC) (ref. 38). Perhaps the selectivity of the two 14-3-3 binding grooves is determined by other complex components, or by conformational changes in 14-3-3 that are induced by the first ligand, to favour binding of the second.

We finally asked whether 14-3-3γ dimerization is relevant for PGC formation. COS7 cells were depleted of 14-3-3γ, transfected with siRNA-resistant replacement vectors that encode wild-type (dimeric) or mutated (monomeric) 14-3-3γ–Flag, and then examined for the formation of PGCs (Fig. 4e,f). The expression of dimeric 14-3-3γ nearly completely rescued PGC formation in 14-3-3γ-depleted cells, whereas the expression of the monomeric 14-3-3γ mutant failed to induce rescue (Fig. 4e,f), which indicates that bridging of BARS and PI(4)KIIIβ by 14-3-3γ is involved in the formation of PGCs.

## 14-3-3γ localizes to the Golgi complex in a BARS- and PI(4)KIIIβ-dependent fashion

We next examined the cellular localization of BARS, PI(4)KIIIβ and 14-3-3γ. Whereas 14-3-3γ (Fig. 5a) and PI(4)KIIIβ localized mostly at the Golgi, BARS seemed diffuse in the cytosol and the nucleus, with detectable, but weak, Golgi enrichment[17] (Fig. 5b,c). We thus sought to clarify the localization of BARS. Prompted by our finding that BARS is recruited to the macropinocytic cup during macropinocytosis[39], we examined whether BARS changes localization during a VSVG traffic pulse. Indeed, BARS was strikingly recruited to the Golgi, including to tubular carrier precursors, during the pulse (Fig. 5d; compare with Fig. 5b and Supplementary Movie S4).

We then analysed whether each of the three components of this complex might affect the location of the others. In 14-3-3γ-depleted cells, BARS–YFP (yellow fluorescent protein) remained at the Golgi, as in normal cells (Supplementary Movies S3 and S4). Thus, although 14-3-3γ depletion prevents BARS-mediated fission, it does not affect BARS localization (Supplementary Movie S3). Similarly, knockdown of 14-3-3γ, or overexpression of 14-3-3γ–Flag, or injection of GST–14-3-3γ, had no effects on the Golgi localization of PI(4)KIIIβ (Supplementary Fig. S3). Thus, 14-3-3γ is not required for localization of BARS and PI(4)KIIIβ. We then examined whether 14-3-3γ at the Golgi might depend on BARS or on PI(4)KIIIβ. The ablation of BARS by siRNAs or by a microinjected anti-BARS antibody resulted in a marked loss of Golgi localization of 14-3-3γ (Fig. 6a–d) and, similarly, knockdown of PI(4)KIIIβ or treatment with brefeldin A (BFA) (PI(4)KIIIβ binding to the Golgi is BFA sensitive)[10] caused redistribution of 14-3-3γ into the cytosol (Fig. 6e-h; and the depletion of both BARS and PI(4)KIIIβ together was moderately more effective than the ablation of each of these two proteins; Supplementary Fig. S4).

The simplest interpretation here is that, although 14-3-3γ can bind to PI(4)KIIIβ and BARS separately, it must interact with both to be efficiently retained at the Golgi (consistent with the theory of a ligand binding to dual sites[40]). A question might be why, if basal Golgi BARS levels are sufficient to localize 14-3-3γ at the Golgi, BARS is further recruited to the Golgi during a traffic pulse. Probably, as the PI(4)KIIIβ–14-3-3γ(2)–BARS complex is likely to assemble/disassemble dynamically, higher levels of Golgi BARS might increase the efficiency of complex formation during intense traffic.

## Mechanism, regulation and function of the BARS–14-3-3γ interaction

Canonical 14-3-3γ binding motifs contain RSXpS/TXP and RXXXpS/TXP sequences (modes I and II, respectively), where R (arginine) and pS/T (phosphorylated serine/threonine) have key roles[35]. In addition, a mode III motif that contains the $pS/TX_{1-2}$–COOH sequence has also been proposed[21]. Thus, although phosphorylation-independent interactions[41] have been reported, 14-3-3 binds preferentially with phosphorylated motifs. For instance, PI(4)KIIIβ binds 14-3-3 through its R291XXS294 sequence, which is phosphorylated by PKD (288-LK**R**TA**S**NP-297; ref. 22), resulting in enhanced basal binding with 14-3-3. We thus searched for 14-3-3 binding sites in BARS. We found two such motifs (http://elm.eu.org), one of which is part of the nucleotide-binding domain (NBD), and can interact with 14-3-3γ (142-GT**R**VQ**S**VE-149; Fig. 7a). We mutated Arg-144 and Ser-147 into alanines (R144A and S147A), and tested whether these mutants ($BARS^{S147A}$ and $BARS^{R144A}$) co-immunoprecipitate co-transfected 14-3-3γ–Flag. Remarkably, 14-3-3γ failed to co-precipitate with these mutants (Fig. 7b and not shown). We then transfected with a plasmid encoding $BARS^{S147A}$–YFP (ref. 39) and monitored the formation of PGCs in live cells. Long carrier precursors emanated from the Golgi, but did not undergo fission (Fig. 7c; Supplementary Movie S5). Thus, Ser-147 in BARS is needed for both the BARS–14-3-3γ interaction and PGC fission.

We next asked whether $BARS^{S147}$ is phosphorylated in Ser-147 *in vivo*, and whether phosphorylation enhances the BARS–14-3-3γ interaction. Here, we used an antibody against phosphorylated Ser-147 in BARS (ref. 39), and calyculin A, a phosphorylated serine/threonine phosphatase inhibitor, to enhance the phosphorylation signal. BARS showed strong phosphorylation in Ser-147, whereas $BARS^{S147A}$ gave no signal (Fig. 7d; lanes 1 and 2). Moreover, calyculin A increased the amount of BARS–YFP that co-precipitated with 14-3-3γ–Flag, but not the (very low) amount of $BARS^{S147A}$ that precipitated with the same 14-3-3γ construct (Fig. 7b). Moreover, calyculin A increased

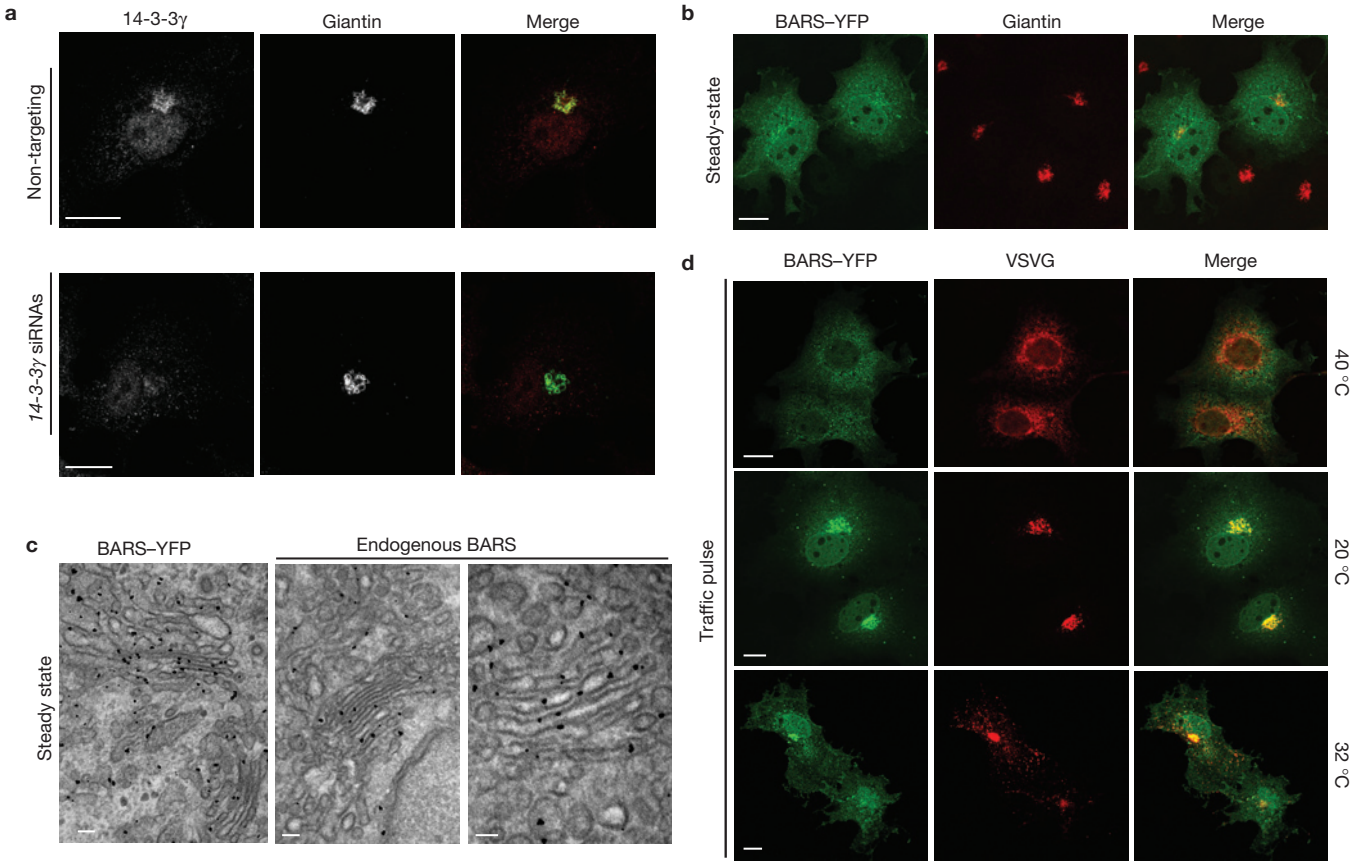


**Figure 5** Localization of 14-3-3γ and BARS. (**a**) Representative confocal microscopy images of COS7 cells transfected with non-targeting (upper panels) or *14-3-3γ* siRNAs (lower panels), fixed and labelled with a polyclonal antibody against 14-3-3γ (red) and with a monoclonal anti-giantin antibody (green; as indicated). Note that in 14-3-3γ-knockdown cells the signal at the Golgi is almost abolished. (**b**) COS7 cells transfected with a plasmid encoding BARS–YFP (total 15 h; green) were fixed at steady state and immunostained with a monoclonal anti-giantin antibody (red). (**c**) Cells transfected with a plasmid encoding BARS–YFP and untransfected cells (endogenous BARS) were immunogold labelled with anti-YFP or anti-CtBP1 monoclonal antibodies, respectively, in EPON sections from COS7 cells. Scale bars, 110 nm (left, centre panels), 140 nm (right panel). (**d**) COS7 cells transfected with a plasmid encoding BARS–YFP (total 15 h; green) were also co-transfected with a plasmid encoding VSVG–CFP for the first 4 h, then subjected to the VSVG TGN-exit assay: 8 h at 40 °C, followed by 3 h at 20 °C and 30 min at 32 °C. Following each stage (40, 20, 32 °C, as indicated), cells were fixed and stained with the P5D4 anti-VSVG antibody (red). Scale bars in **a**,**b**,**d**, 10 μm.

the affinity of BARS for recombinant GST–14-3-3γ (Fig. 7e). Notably, under these conditions, calyculin A does not affect PGC formation (Supplementary Fig. S5). Thus, phosphorylation of BARS in Ser-147 enhances its interaction with 14-3-3γ.

The PAK 1–3 kinases (here collectively referred to as PAK, for brevity) co-precipitated with BARS (Fig. 1e) and can phosphorylate BARS in Ser-147 (ref. 42). Moreover, this PAK-induced phosphorylation activates BARS-dependent fission of macropinosomes[39]. We thus examined the effect of PAK on BARS *in vivo*, using the PAK-AID (autoinhibitory domain) as a specific inhibitor[27,43]. Overexpressed BARS gave a phosphorylation signal (whereas $BARS^{S147A}$ did not) that was inhibited by co-expression of the AID (Fig. 7d). We then tested whether PAK localizes at the Golgi and is required for PGC formation. Whereas at steady state PAK showed a diffuse cytosolic distribution, it was strikingly recruited to the Golgi during a VSVG traffic pulse (Supplementary Figs S6 and S7), as previously shown for BARS (Fig. 5b,d). We then inhibited PAK by (1) microinjection of a neutralizing antibody against PAK1–3 (ref. 44), (2) use of the specific blocker of PAK1–3, 2, 2′-dihydroxy-1, 1′-dinaphthyldisulphide (IPA-3) (ref. 45), (3) transfection with a plasmid encoding the PAK-AID[27,43] and (4) use of siRNAs against PAK1, PAK2 and PAK3 (Fig. 7f and Supplementary Fig. S8). The antibody and the PAK1–3 blocker IPA-3 reduced PGC formation by 70%, whereas expression of the AID or depletion of PAK1 (but not of PAK2 and PAK3) reduced PGCs by 30% (Fig. 7f) and VSVG arrival at the plasma membrane (Supplementary Fig. S8b; none of the siRNAs affected the organization of the Golgi; Supplementary Fig. S8c). Perhaps these latter two treatments are less effective because they inhibit PAK incompletely, or because they allow enough time for functional compensation to take place. Regardless, the simplest interpretation of these data is that phosphorylation by PAK of Ser-147 in BARS enhances the BARS–14-3-3γ interaction and facilitates PGC fission.

Notably, components of the BARS complex are involved in fission at other traffic steps[17,39,46–52]. For instance, BARS and PAK1 are required for macropinocytosis[39] and BARS for COPI vesicle fission[46]. We thus examined the role of 14-3-3γ, PI(4)KIIIβ and PAK1 in macropinocytosis and in COPI-dependent retrograde trafficking. Here, 14-3-3γ is involved in both, PAK1 in macropinocytosis and PI(4)KIIIβ in neither (Fig. 8a,b). Thus, BARS and 14-3-3γ are common players in the three fission processes examined so far. Possibly, 14-3-3γ

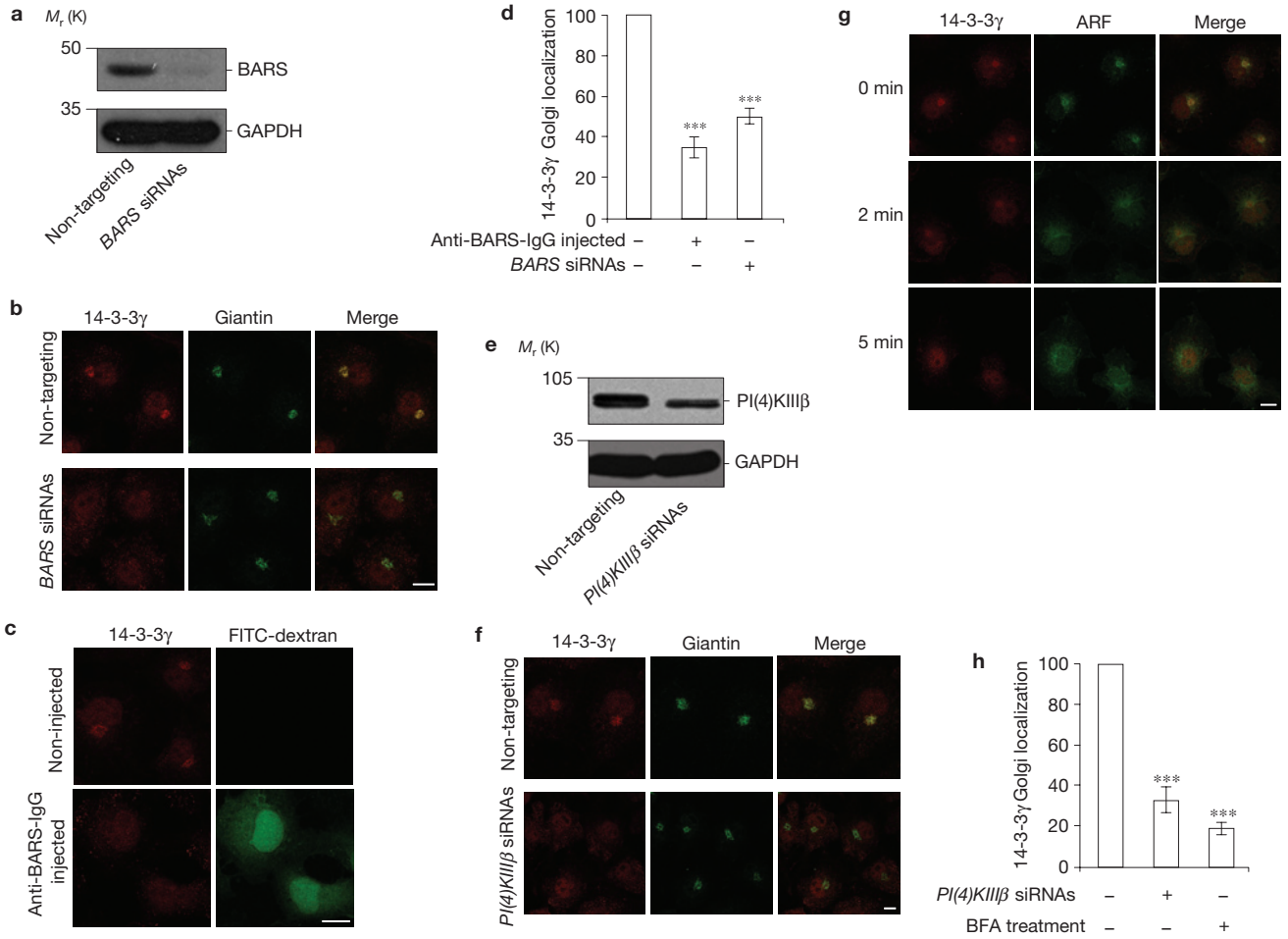


**Figure 6** BARS and PI(4)KIIIβ are required for Golgi localization of 14-3-3γ. (**a**) Representative immunoblotting of COS7 cells treated with non-targeting siRNAs or *BARS*-directed siRNAs, and processed for immunoblotting of BARS knockdown, with antibodies against BARS and GAPDH. (**b**) Representative images of cells from **a**, labelled with a polyclonal antibody against 14-3-3γ (red) and with a monoclonal anti-giantin antibody (green, Golgi marker) to identify cells positive for 14-3-3γ in the Golgi area. (**c**) Representative images of COS7 cells microinjected with an anti-BARS antibody (1.0–1.5 mg ml$^{-1}$; anti-BARS-IgG injection) together with fluorescent dextran as injection marker (fluorescein isothiocyanate, FITC-dextran; green). Cells were fixed 15–18 h after injection and labelled with a polyclonal antibody against 14-3-3γ (red). 14-3-3γ Golgi localization was not affected by injection of a preimmune IgG (data not shown). (**d**) Quantification of 14-3-3γ Golgi localization as shown in **b**,**c**. (**e**) Representative immunoblotting of COS7 cells treated with non-targeting siRNAs or *PI(4)KIIIβ*-directed siRNAs, and processed for immunoblotting of PI(4)KIIIβ knockdown, with antibodies against PI(4)KIIIβ and GAPDH. (**f**) Representative images of cells from **e**, labelled with a polyclonal antibody against 14-3-3γ (red) and with a monoclonal anti-giantin antibody (green, Golgi marker) to identify cells positive for 14-3-3γ in the Golgi area. (**g**) Representative images of COS7 cells treated with 1 μg ml$^{-1}$ BFA for 0, 2 and 5 min, to induce redistribution of ARF from Golgi membranes, as described[10], fixed and labelled with both an anti-ARF antibody, to follow BFA-treated cells, and an anti-14-3-3γ antibody, to follow 14-3-3γ Golgi localization. (**h**) Quantification of 14-3-3γ Golgi localization as shown in **f**–**g**. Scale bars in **b**,**c**,**f**,**g**, 10 μm. Data in **d**,**h** are means ± s.d. of three independent experiments. $^{***}P < 0.005$ (Student's *t*-test). Uncropped images of blots are shown in Supplementary Fig. S9.2.

links BARS to the machineries involved in these transport steps, and perhaps also facilitates the active conformation of BARS (ref. 53) (for instance, the active conformation of PI(4)KIIIβ is stabilized by 14-3-3s; ref. 22).

### PI(4)KIIIβ–14-3-3γ(2)–BARS forms *in vivo* at the Golgi complex during trafficking

Finally, we tested whether the BARS–14-3-3γ interaction occurs at the Golgi *in vivo*. For this, we carried out fluorescence resonance energy transfer (FRET)-based experiments, by both acceptor photobleaching FRET (apFRET) and fluorescence lifetime imaging microscopy FRET (FLIM-FRET), using PI(4)KIIIβ–CFP (cyan fluorescent protein) as the FRET donor, and BARS–YFP as the FRET acceptor (Fig. 8c–g). As a positive control, we used a CFP–Epac–YFP fusion construct that shows clear FRET when expressed in mammalian cells[54].

We first used the apFRET approach both at steady state and during a VSVG traffic pulse. A significant (although moderate) FRET effect was detected over the Golgi area, but not in the cytosol or nucleus (Fig. 8c–e); moreover, the FRET efficiency in the Golgi (Fig. 8d) increased during active trafficking (Fig. 8e; in line with the recruitment of BARS to the Golgi during a traffic pulse; Fig. 5b,d and Supplementary Figs S6 and S7). As a control, we measured FRET in cells co-expressing PI(4)KIIIβ and a point mutant of BARS (BARS$^{S147A}$) that localizes to the Golgi but cannot interact with 14-3-3γ (Fig. 7b,c). Here, FRET at the Golgi was negligible (Fig. 8e). As a

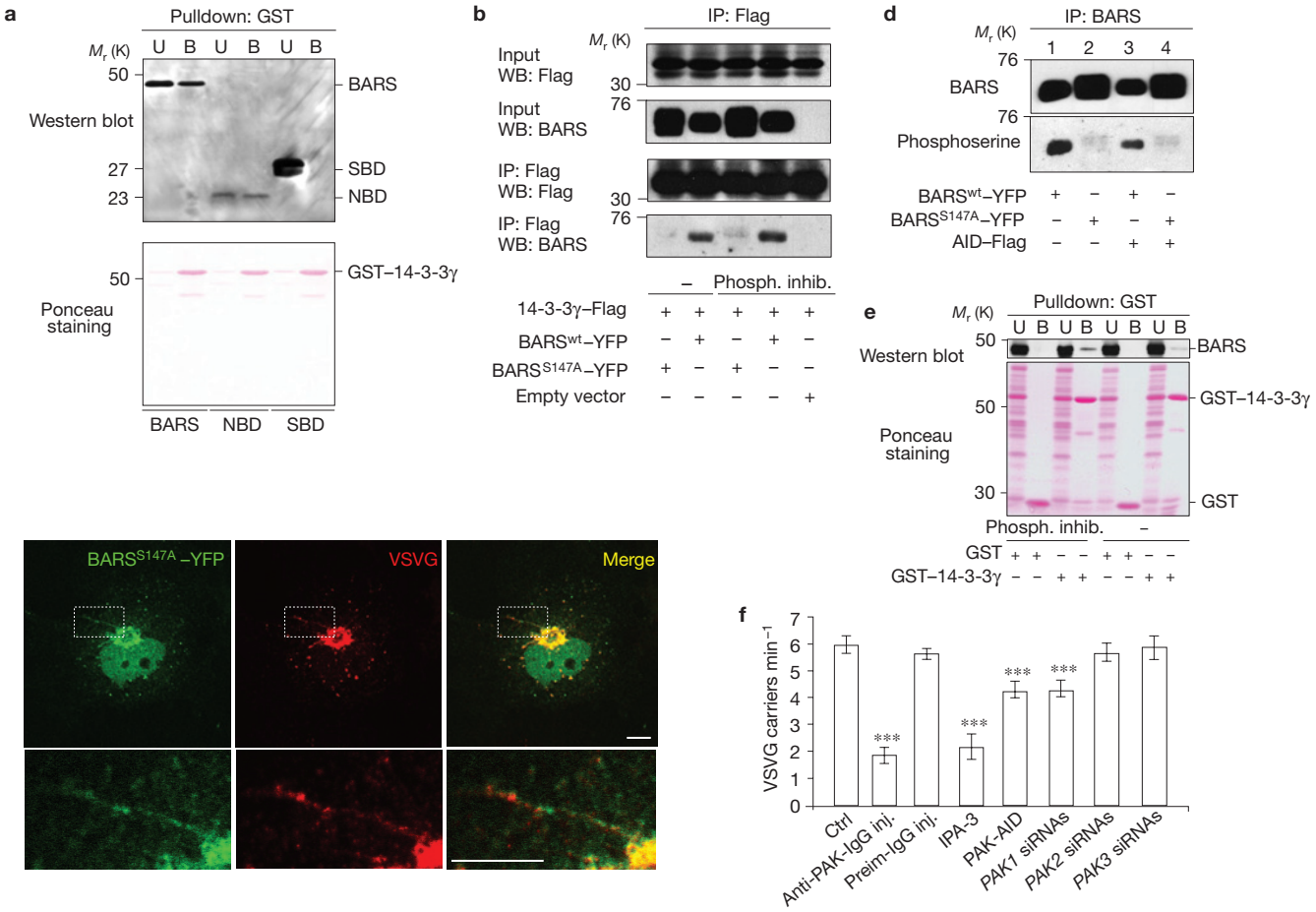


**Figure 7** Molecular organization, regulation and functional role of BARS–14-3-3γ interaction. (**a**) GST pulldown assays of GST–14-3-3γ with equimolar recombinant His–BARS, 50 μg, His–NBD, 23 μg or His–SBD (substrate-binding domain), 27 μg. Unbound (U) and bound (B) proteins analysed. Top: Western blotting using an anti-His antibody. Bottom: Ponceau-S staining. No His-tagged proteins were eluted with recombinant GST (data not shown). (**b**) Representative immunoprecipitation (IP) with anti-Flag antibody of lysates from COS7 cells transfected with plasmids encoding 14-3-3γ–Flag and BARS$^{wt}$–YFP, BARS$^{S147A}$–YFP or empty vector, and incubated without (–) or with (Phosph. inhib.) calyculin A for 10 min. Western blotting (WB) with anti-Flag and polyclonal anti-BARS antibodies: total lysate (input) and Flag-immunoprecipitated proteins (IP: Flag). (**c**) Confocal microscopy images of BARS$^{S147A}$–YFP-expressing COS7 cell infected with VSV and subjected to TGN-exit assay with 0.5% tannic acid. Cells were fixed after 30 min at 32 °C and labelled with P5D4 anti-VSVG antibody (red) for formation of PGCs and PGC precursors. Bottom panels: magnification of tubular carrier precursor. Scale bars, 5 μm. (**d**) Representative immunoprecipitation (IP) with anti-BARS polyclonal antibody of COS7 cells transfected with BARS$^{wt}$–YFP or BARS$^{S147A}$–YFP in the absence (lanes 1, 2) and presence (lanes 3, 4) of PAK-AID–Flag. Western blotting with an anti-phosphoserine antibody to reveal the PAK1-dependent phosphorylation state of BARS (ref. 39) (bottom). The blot was reprobed with an anti-YFP antibody for immunoprecipitated proteins (top). (**e**) GST pulldown assay of GST (30 μg) and GST–14-3-3γ (55 μg), of control (–) and calyculin-A-treated (Phosph. inhib.) lysates from COS7 cells. Unbound (U) and bound (B) proteins analysed. Top: Western blotting using an anti-BARS antibody. Bottom: Ponceau-S staining. (**f**) Quantification of VSVG-containing PGCs in untreated (Ctrl) and treated COS7 cells, as indicated: transfected with PAK-AID for 24 h, or *PAK1, PAK2, PAK3* siRNAs for 48 h, before VSV infection, or microinjected (inj.) with anti-PAK-IgG (C-19) or with preimmune IgG (1 mg ml$^{-1}$ after 1 h at 20 °C), or treated with IPA-3 (15 μM, 30 min, 32 °C), during TGN-exit assay with 0.5% tannic acid. After the TGN-exit assay, cells were immunostained with the P5D4 anti-VSVG antibody, plus respective treatment-relevant conditions: anti-Flag antibody for PAK-AID-expressing cells, anti-PAK antibodies for interference efficiency for *PAK1, PAK2, PAK3* siRNAs, secondary anti-rabbit antibody for anti-PAK-IgG- and preimmune-IgG-microinjected cells, and anti-phospho-PAK1/2/3 [pThr423] antibody for inhibition of PAK by IPA-3. Data are means ± s.d. of three independent experiments. $^{***}P < 0.005$ (Student's *t*-test). Uncropped images of blots are shown in Supplementary Fig. S9.2.

further control, we used the trans-Golgi enzyme galactosyltransferase (GalT–CFP). No FRET was seen in cells co-expressing GalT–CFP and BARS–YFP (not shown). We also used the FLIM-FRET approach. Here again, when PI(4)KIIIβ–CFP and BARS–YFP were co-expressed in COS7 cells, significant FRET was observed (Fig. 8f,g), whereas no FRET was detected between the mutant BARS$^{S147A}$–YFP and PI(4)KIIIβ–CFP (Fig. 8g).

As noted, the average FRET efficiency over the Golgi was modest. We reasoned that the BARS–PI(4)KIIIβ complex should form only in Golgi regions that are involved in carrier formation, rather than uniformly over the organelle. Indeed, examination of the distribution of FRET in the Golgi area showed that FRET occurs only at a few 'hot spots', whereas in other areas FRET is negligible (Fig. 8d). Quantification confirmed that the FRET effect is intense only in a few small Golgi regions (Fig. 8d), presumably where PGCs are forming.

In conclusion here, apFRET and FLIM-FRET indicate that PI(4)KIIIβ and BARS form a complex *in vivo*, and that this effect is enhanced during a VSVG traffic pulse.

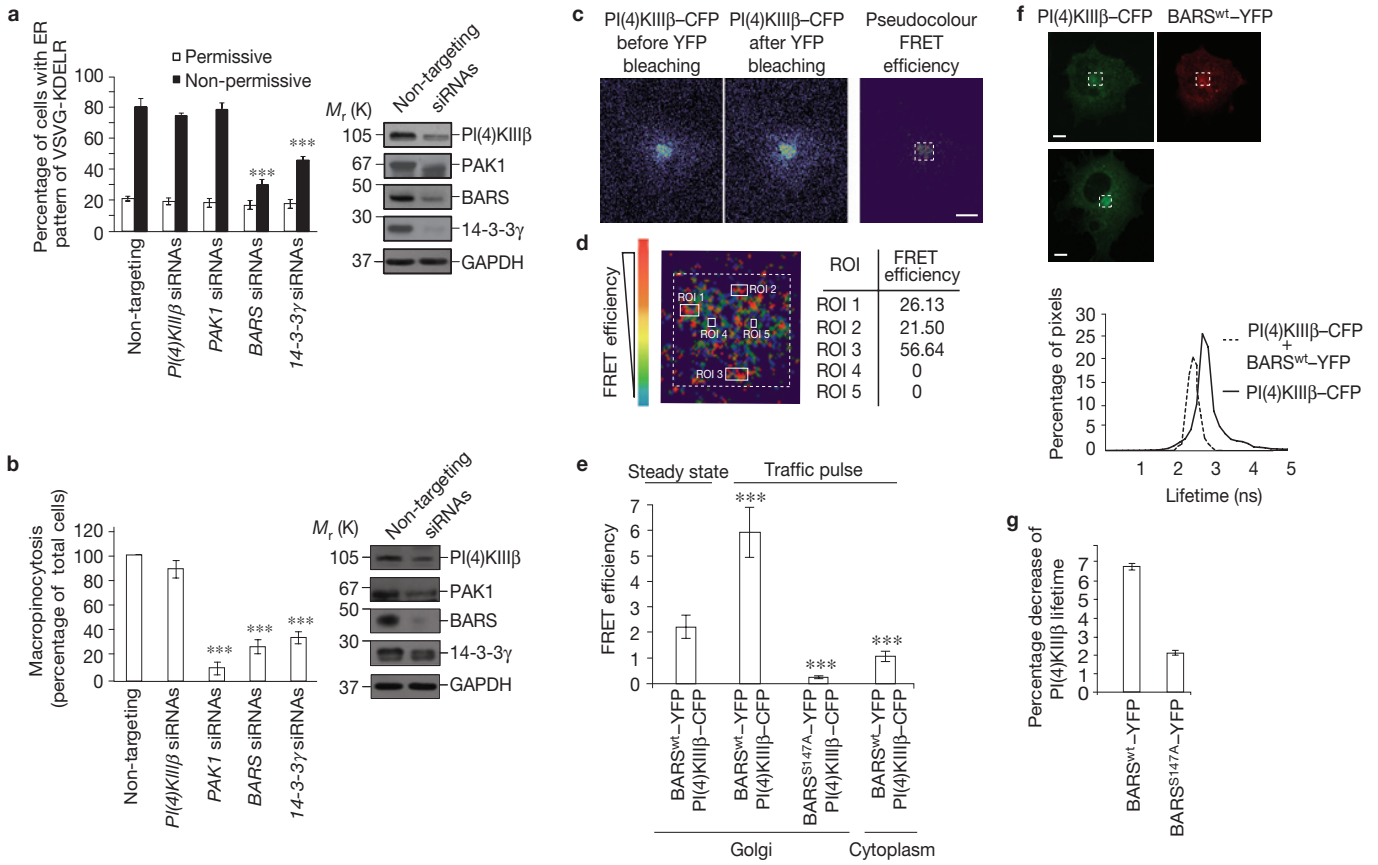


**Figure 8** 14-3-3γ is required for COPI retrograde transport and macropinocytosis, and close association of PI(4)KIIIβ and BARS at the Golgi during a traffic pulse. (**a**,**b**) COS7 (**a**) and A431 (**b**) cells treated with non-targeting siRNAs or *PI(4)KIIIβ-*, *PAK1-*, *BARS-* or *14-3-3γ*-directed siRNAs. Left: Quantification of COPI-dependent retrograde transport (redistribution of VSVG-KDELR (KDEL receptor) from Golgi to endoplasmic reticulum (ER), as described[46]; **a**), and macropinocytosing cells (as described[39]; **b**). Data are means ± s.d. of three independent experiments. Right: Efficiency of knockdown by western blotting of cell lysates (specific antibodies as indicated). (**c**–**g**) FRET of COS7 cells transfected with PI(4)KIIIβ–CFP plus BARS$^{wt}$–YFP (**c**–**g**) or BARS$^{S147A}$–YFP (**e**,**g**). Cells were subjected to a VSVG traffic pulse before fixing (unless otherwise indicated). (**c**) Representative apFRET pseudocolour images of PI(4)KIIIβ–CFP fluorescence intensity before and after whole-cell bleaching of BARS$^{wt}$–YFP fluorescence (left, middle) and pseudocolour map of apFRET efficiency (right). (**d**) Enlarged pseudocolour map (left) of Golgi area in **c** (right, dashed square), showing regions of interest (ROIs; white boxes) and colour-coded FRET efficiency scale for quantification (right, Table). (**e**) Quantification of apFRET efficiency illustrated in **c**,**d** under conditions indicated, for Golgi area and cytoplasm, and at steady state and during a VSVG traffic pulse. Data are means ± s.d. ($n = 20$ cells/condition). (**f**) Representative FLIM-FRET images of cells (top two, green, PI(4)KIIIβ–CFP; red, BARS$^{wt}$–YFP; bottom one, green, PI(4)KIIIβ–CFP alone). The fluorescence lifetime of PI(4)KIIIβ–CFP is measured in the Golgi area (dashed rectangle). Bottom graph: Distribution of fluorescence lifetime for PI(4)KIIIβ–CFP alone and with BARS$^{wt}$–YFP (Methods), showing shift towards shorter lifetimes (hence indicating FRET) with co-expression with BARS$^{wt}$–YFP. The average fluorescence lifetimes of PI(4)KIIIβ–CFP calculated for more than 15 cells were 2.36 ns (PI(4)KIIIβ–CFP alone) and 2.21 ns (with BARS$^{wt}$–YFP). (**g**) Quantification of FLIM-FRET efficiency (percentage decrease in PI(4)KIIIβ–CFP lifetime) illustrated in **f**, under conditions indicated. Data are means ± s.d. ($n = 15$ cells/condition). (**a**,**b**,**e**) $^{***}P < 0.005$ (Student's $t$-test), versus non-targeting siRNAs (**a**,**b**) and steady-state control (**e**). Scale bars in **c**,**f**, 10 μm. Uncropped images of blots are shown in Supplementary Fig. S9.3.

## DISCUSSION

This study describes a multiprotein complex that is required for generation of basolaterally directed PGCs. This multiprotein complex comprises a core consisting of BARS and PI(4)KIIIβ bridged by a 14-3-3γ dimer, and of further partners including ARF, NCS-1, PKD and PAK (Fig. 1e). On the basis of previous knowledge as well as of current data, we suggest the following scenario for the assembly of these components: first there will be the activation of ARF at the Golgi, which induces recruitment and activation of PI(4)KIIIβ, to stimulate PtdIns4P synthesis[10]. ARF also interacts with PKD (ref. 55) and NCS-1 (ref. 7), both of which enhance the synthesis of PtdIns4P by further activating PI(4)KIIIβ (refs 25,26). Together with ARF, PtdIns4P recruits FAPP2 (refs 9,11,12), which can lead to membrane bending and tubulation[12,56–58] (see refs 9,11,59 for a discussion of the basolateral versus apical role of FAPP2). On phosphorylation by PKD, PI(4)KIIIβ also binds to 14-3-3γ (ref. 22), a dimeric protein adapter that, in turn, binds to BARS at the Golgi surface. This interaction is stabilized/enhanced by phosphorylation by PAK, and it results in formation of a PI(4)KIII β–14-3-3γ(2)–BARS core complex. Importantly, this complex forms selectively at the Golgi during trafficking, as indicated by *in vivo* FRET-based imaging microscopy (Fig. 8c–g).

What is the function of the PI(4)KIIIβ–14-3-3γ(2)–BARS complex? Manipulations that disrupt it result in elongated carrier precursors that do not undergo fission (Figs 2d, 7c and Supplementary Movies S2, S3 and S5). Considering that PI(4)KIIIβ (with its activator and effector molecules ARF, NCS-1, PtdIns4P, FAPP2) is involved in initiation of carrier formation, whereas BARS and its interactors (for example, PLD

(ref. 51); see below) operate in fission[17,46], a key function of the complex seems to be the linking of the fission machinery to the site of tubule budding. Thus, the observed fission-defective tubulation phenotype would result from unlinking of the carrier budding and fission processes.

A remaining question is how, once in the complex, BARS might ultimately act to induce fission. Although this is beyond the scope of the present study, we note that, on the basis of its structure[18], BARS is unlikely to have any mechano-enzymatic activity. Rather, the available data indicate that BARS might function as a scaffold, to assemble into the fission complex lipid-metabolizing enzymes such as PI(4)KIIIβ, PLD1 (ref. 51) and possibly acyltransferases[46,47,60], presumably to generate a local lipid environment that favours fission. Of note here is that the CtBP2 isoform of the CtBP/BARS family, RIBEYE, has been recently found to be a lysophosphatidic acid acyltransferase[61] (see also refs 62,63).

A final question concerns the mechanisms by which ARF, PKD and PAK are activated to generate this complex. Each of these proteins is a target of complex regulatory inputs. We have previously proposed that traffic from the endoplasmic reticulum to the Golgi complex triggers a signalling cascade on the Golgi complex itself[64]. It is possible that this cascade can promote activation of these kinases, thus coordinating the arrival and departure of cargo in and out of the Golgi complex. □

## METHODS

Methods and any associated references are available in the online version of the paper at www.nature.com/naturecellbiology

*Note: Supplementary Information is available on the Nature Cell Biology website*


### ACKNOWLEDGEMENTS

The authors would like to thank all colleagues who kindly provided them with antibodies and reagents (as listed under 'Reagents'); M. A. De Matteis and C. Wilson for critical reading of the manuscript; J. Chernoff for the PAK inhibitor IPA-3 (Fox Chase Cancer Center); C. P. Berrie for critical reading of and editorial assistance with the manuscript; C. Cericola for preparation of the anti-BARS antibody; R. Le Donne and E. Fontana for preparation of the figures; the Integrated Microscopy Facility at the Institute of Genetics and Biophysics, National Research Council, Naples, and the Dynamic Imaging Microscopy Facility at the CEINGE Institute, Naples, for support in imaging microscopy, data processing and analysis; the Italian Association for Cancer Research (to D.C. IG4664 and IG10341, to A.L. IG4700, to A.C. IG6074 and to R.S.P. IG10233), Telethon Italia (to D.C. GGPO9274, to A.L. GGPO8231 and to R.S.P. GTF08001), the European Community Seventh Framework Programme FP7/2007-2013 HEALTH-F2-2007-201804 (Eucilia to A.L.), grant FIT DM 24/09/2009, Legge 46/82, and FaReBio, Ministry of Economy and Finance (to D.C.) for financial support. C.V., A.P. and S.S. were recipients of Italian Foundation for Cancer Research Fellowships (FIRC, Milan, Italy).


### AUTHOR CONTRIBUTIONS

C.V. designed, carried out and analysed all of the experiments and co-wrote the manuscript. G.T. carried out immunofluorescence and electron microscopy experiments. A.P. carried out COPI retrograde transport and macropinocytosis assays. G.D.T., M.S. and D.P. produced essential antibodies. F.F. carried out FRET and FLIM experiments. S.S. carried out initial experiments. R.G. carried out some phosphorylation experiments. R.S.P. carried out time-lapse microscopy. A.C. and S.M. contributed to relevant discussions and suggestions. D.C. and A.L. conceived and supervised the project, discussed and analysed the data and co-wrote the manuscript.

### COMPETING FINANCIAL INTERESTS

The authors declare no competing financial interests.


Published online at www.nature.com/naturecellbiology
Reprints and permissions information is available online at www.nature.com/reprints



1. De Matteis, M. A. & Luini, A. Exiting the Golgi complex. *Nat. Rev. Mol. Cell Biol.* **9,** 273–284 (2008).
2. Hirschberg, K. *et al.* Kinetic analysis of secretory protein traffic and characterization of golgi to plasma membrane transport intermediates in living cells. *J. Cell Biol.* **143,** 1485–1503 (1998).
3. Polishchuk, E. V., Di Pentima, A., Luini, A. & Polishchuk, R. S. Mechanism of constitutive export from the golgi: bulk flow via the formation, protrusion, and en bloc cleavage of large trans-golgi network tubular domains. *Mol. Biol. Cell* **14,** 4470–4485 (2003).
4. Rodriguez-Boulan, E., Kreitzer, G. & Musch, A. Organization of vesicular trafficking in epithelia. *Nat. Rev. Mol. Cell Biol.* **6,** 233–247 (2005).
5. Rothman, J. E. Lasker Basic Medical Research Award. The machinery and principles of vesicle transport in the cell. *Nat. Med.* **8,** 1059–1062 (2002).
6. Schekman, R. Lasker Basic Medical Research Award. SEC mutants and the secretory apparatus. *Nat. Med.* **8,** 1055–1058 (2002).
7. Haynes, L. P., Thomas, G. M. & Burgoyne, R. D. Interaction of neuronal calcium sensor-1 and ADP-ribosylation factor 1 allows bidirectional control of phosphatidylinositol 4-kinase β and trans-Golgi network–plasma membrane traffic. *J. Biol. Chem.* **280,** 6047–6054 (2005).
8. Bruns, J. R., Ellis, M. A., Jeromin, A. & Weisz, O. A. Multiple roles for phosphatidylinositol 4-kinase in biosynthetic transport in polarized Madin-Darby canine kidney cells. *J. Biol. Chem.* **277,** 2012–2018 (2002).
9. Godi, A. *et al.* FAPPs control Golgi-to-cell-surface membrane traffic by binding to ARF and PtdIns(4)P. *Nat. Cell Biol.* **6,** 393–404 (2004).
10. Godi, A. *et al.* ARF mediates recruitment of PtdIns-4-OH kinase-β and stimulates synthesis of PtdIns(4,5)P2 on the Golgi complex. *Nat. Cell Biol.* **1,** 280–287 (1999).
11. D'Angelo, G. *et al.* Glycosphingolipid synthesis requires FAPP2 transfer of glucosylceramide. *Nature* **449,** 62–67 (2007).
12. Cao, X. *et al.* Golgi protein FAPP2 tubulates membranes. *Proc. Natl Acad. Sci. USA* **106,** 21121–21125 (2009).
13. Diaz Anel, A. M. Phospholipase C β 3 is a key component in the Gβγ/PKCη/PKD-mediated regulation of trans-Golgi network to plasma membrane transport. *Biochem. J.* **406,** 157–165 (2007).
14. Liljedahl, M. *et al.* Protein kinase D regulates the fission of cell surface destined transport carriers from the trans-Golgi network. *Cell* **104,** 409–420 (2001).
15. Yeaman, C. *et al.* Protein kinase D regulates basolateral membrane protein exit from trans-Golgi network. *Nat. Cell Biol.* **6,** 106–112 (2004).
16. Miserey-Lenkei, S. *et al.* Rab and actomyosin-dependent fission of transport vesicles at the Golgi complex. *Nat. Cell Biol.* **12,** 645–654 (2010).
17. Bonazzi, M. *et al.* CtBP3/BARS drives membrane fission in dynamin-independent transport pathways. *Nat. Cell Biol.* **7,** 570–580 (2005).
18. Nardini, M. *et al.* CtBP/BARS: a dual-function protein involved in transcription co-repression and Golgi membrane fission. *EMBO J.* **22,** 3122–3130 (2003).
19. Corda, D., Colanzi, A. & Luini, A. The multiple activities of CtBP/BARS proteins: the Golgi view. *Trends Cell Biol.* **16,** 167–173 (2006).
20. Colanzi, A. & Corda, D. Mitosis controls the Golgi and the Golgi controls mitosis. *Curr. Opin. Cell Biol.* **19,** 386–393 (2007).
21. Aitken, A. 14-3-3 proteins: a historic overview. *Semin. Cancer Biol.* **16,** 162–172 (2006).
22. Hausser, A. *et al.* Phospho-specific binding of 14-3-3 proteins to phosphatidylinositol 4-kinase III β protects from dephosphorylation and stabilises lipid kinase activity. *J. Cell Sci.* **119,** 3613–3621 (2006).
23. Demmel, L. *et al.* Nucleocytoplasmic shuttling of the Golgi phosphatidylinositol 4-kinase Pik1 is regulated by 14-3-3 proteins and coordinates Golgi function with cell growth. *Mol. Biol. Cell* **19,** 1046–1061 (2008).
24. Valente, C., Spanò, S., Luini, A. & Corda, D. Purification and functional properties of the membrane fissioning protein CtBP3/BARS. *Methods Enzymol.* **404,** 296–316 (2005).
25. Zhao, X. *et al.* Interaction of neuronal calcium sensor-1 (NCS-1) with phosphatidylinositol 4-kinase β stimulates lipid kinase activity and affects membrane trafficking in COS-7 cells. *J. Biol. Chem.* **276,** 40183–40189 (2001).
26. Hausser, A. *et al.* Protein kinase D regulates vesicular transport by phosphorylating and activating phosphatidylinositol-4 kinase IIIβ at the Golgi complex. *Nat. Cell Biol.* **7,** 880–886 (2005).
27. Eswaran, J., Soundararajan, M., Kumar, R. & Knapp, S. UnPAKing the class differences among p21-activated kinases. *Trends Biochem. Sci.* **33,** 394–403 (2008).
28. Rodriguez Boulan, E. & Pendergast, M. Polarized distribution of viral envelope proteins in the plasma membrane of infected epithelial cells. *Cell* **20,** 45–54 (1980).
29. Matlin, K. S. & Simons, K. Reduced temperature prevents transfer of a membrane glycoprotein to the cell surface but does not prevent terminal glycosylation. *Cell* **34,** 233–243 (1983).
30. Polishchuk, R., Di Pentima, A. & Lippincott-Schwartz, J. Delivery of raft-associated, GPI-anchored proteins to the apical surface of polarized MDCK cells by a transcytotic pathway. *Nat. Cell Biol.* **6,** 297–307 (2004).
31. Marra, P. *et al.* The GM130 and GRASP65 Golgi proteins cycle through and define a subdomain of the intermediate compartment. *Nat. Cell Biol.* **3,** 1101–1113 (2001).
32. Pelkmans, L. & Helenius, A. Insider information: what viruses tell us about endocytosis. *Curr. Opin. Cell Biol.* **15,** 414–422 (2003).
33. Steinacker, P. *et al.* Unchanged survival rates of 14-3-3γ knockout mice after inoculation with pathological prion protein. *Mol. Cell Biol.* **25,** 1339–1346 (2005).

34. Chaudhri, M., Scarabel, M. & Aitken, A. Mammalian and yeast 14-3-3 isoforms form distinct patterns of dimers *in vivo*. *Biochem. Biophys. Res. Commun.* **300,** 679–685 (2003).
35. Yaffe, M. B. *et al.* The structural basis for 14-3-3:phosphopeptide binding specificity. *Cell* **91,** 961–971 (1997).
36. Braselmann, S. & McCormick, F. Bcr and Raf form a complex *in vivo* via 14-3-3 proteins. *EMBO J.* **14,** 4839–4848 (1995).
37. Vincenz, C. & Dixit, V. M. 14-3-3 proteins associate with A20 in an isoform-specific manner and function both as chaperone and adapter molecules. *J. Biol. Chem.* **271,** 20029–20034 (1996).
38. Van Der Hoeven, P. C., Van Der Wal, J. C., Ruurs, P., Van Dijk, M. C. & Van Blitterswijk, J. 14-3-3 isotypes facilitate coupling of protein kinase C-ζ to Raf-1: negative regulation by 14-3-3 phosphorylation. *Biochem. J.* **345 Pt 2,** 297–306 (2000).
39. Liberali, P. *et al.* The closure of Pak1-dependent macropinosomes requires the phosphorylation of CtBP1/BARS. *EMBO J.* **27,** 970–981 (2008).
40. Liu, D. *et al.* Crystal structure of the ζ isoform of the 14-3-3 protein. *Nature* **376,** 191–194 (1995).
41. Ottmann, C. *et al.* Phosphorylation-independent interaction between 14-3-3 and exoenzyme S: from structure to pathogenesis. *EMBO J.* **26,** 902–913 (2007).
42. Barnes, C. J. *et al.* Functional inactivation of a transcriptional corepressor by a signaling kinase. *Nat. Struct. Biol.* **10,** 622–628 (2003).
43. Dharmawardhane, S. *et al.* Regulation of macropinocytosis by p21-activated kinase-1. *Mol. Biol. Cell* **11,** 3341–3352 (2000).
44. Paglini, G., Peris, L., Diez-Guerra, J., Quiroga, S. & Caceres, A. The Cdk5-p35 kinase associates with the Golgi apparatus and regulates membrane traffic. *EMBO Rep.* **2,** 1139–1144 (2001).
45. Deacon, S. W. *et al.* An isoform-selective, small-molecule inhibitor targets the autoregulatory mechanism of p21-activated kinase . *Chem. Biol.* **15,** 322–331 (2008).
46. Yang, J. S. *et al.* A role for BARS at the fission step of COPI vesicle formation from Golgi membrane. *EMBO J.* **24,** 4133–4143 (2005).
47. Yang, J. S. *et al.* COPI acts in both vesicular and tubular transport. *Nat. Cell Biol.* **13,** 996–1003 (2011).
48. Hidalgo Carcedo, C. *et al.* Mitotic Golgi partitioning is driven by the membrane-fissioning protein CtBP3/BARS. *Science* **305,** 93–96 (2004).
49. Colanzi, A. *et al.* The Golgi mitotic checkpoint is controlled by BARS-dependent fission of the Golgi ribbon into separate stacks in G2. *EMBO J.* **26,** 2465–2476 (2007).
50. Saeed, M. F., Kolokoltsov, A. A., Albrecht, T. & Davey, R. A. Cellular entry of ebola virus involves uptake by a macropinocytosis-like mechanism and subsequent trafficking through early and late endosomes. *PLoS Pathog.* **6,** e1001110 (2010).
51. Haga, Y., Miwa, N., Jahangeer, S., Okada, T. & Nakamura, S. CtBP1/BARS is an activator of phospholipase D1 necessary for agonist-induced macropinocytosis. *EMBO J.* **28,** 1197–1207 (2009).
52. Moreau, D. *et al.* Genome-wide RNAi screens identify genes required for ricin and PE intoxications. *Dev. Cell* **21,** 231–244 (2011).
53. Tzivion, G. & Avruch, J. 14-3-3 proteins: active cofactors in cellular regulation by serine/threonine phosphorylation. *J. Biol. Chem.* **277,** 3061–3064 (2002).
54. Ponsioen, B. *et al.* Detecting cAMP-induced Epac activation by fluorescence resonance energy transfer: Epac as a novel cAMP indicator. *EMBO Rep.* **5,** 1176–1180 (2004).
55. Pusapati, G. V. *et al.* Role of the second cysteine-rich domain and Pro275 in PKD2 interaction with ARF1, TGN recruitment and protein transport. *Mol. Biol. Cell* **21,** 1011–1022 (2010).
56. Beck, R. *et al.* Membrane curvature induced by Arf1-GTP is essential for vesicle formation. *Proc. Natl Acad. Sci. USA* **105,** 11731–11736 (2008).
57. Krauss, M. *et al.* Arf1-GTP-induced tubule formation suggests a function of Arf family proteins in curvature acquisition at sites of vesicle budding. *J. Biol. Chem.* **283,** 27717–27723 (2008).
58. Lundmark, R., Doherty, G. J., Vallis, Y., Peter, B. J. & McMahon, H. T. Arf family GTP loading is activated by, and generates, positive membrane curvature. *Biochem. J.* **414,** 189–194 (2008).
59. Vieira, O. V., Verkade, P., Manninen, A. & Simons, K. FAPP2 is involved in the transport of apical cargo in polarized MDCK cells. *J. Cell Biol.* **170,** 521–526 (2005).
60. Schmidt, J. A. & Brown, W. J. Lysophosphatidic acid acyltransferase 3 regulates Golgi complex structure and function. *J. Cell Biol.* **186,** 211–218 (2009).
61. Schwarz, K., Natarajan, S., Kassas, N., Vitale, N. & Schmitz, F. The synaptic ribbon is a site of phosphatidic acid generation in ribbon synapses. *J. Neurosci.* **31**, 15996–16011 (2011).
62. Weigert, R. *et al.* CtBP/BARS induces fission of Golgi membranes by acylating lysophosphatidic acid. *Nature* **402,** 429–433 (1999).
63. Gallop, J. L., Butler, P. J. & McMahon, H. T. Endophilin and CtBP/BARS are not acyl transferases in endocytosis or Golgi fission. *Nature* **438,** 675–678 (2005).
64. Pulvirenti, T. *et al.* A traffic-activated Golgi-based signalling circuit coordinates the secretory pathway. *Nat. Cell Biol.* **10,** 912–922 (2008).

## METHODS

**Reagents.** The p50-2 rabbit polyclonal (1:1,000 Western blot (WB); 1:50 immunofluorescence (IF) dilution) and BC3 mouse monoclonal 1:100 (WB) anti-BARS antibodies were raised against GST–BARS (refs 24,65). Antibodies and reagents provided as follows: anti-p75 extracellular domain, L.F. Reichardt (University of California); anti-VSVG lumenal domain 1:2,000 (IF), anti-PI(4)KIIIβ 1:500 (IF), 1:10,000 (WB); anti-ARF1 1:5,000 (WB); anti-NCS-1 1:1,000 (WB); anti-giantin 1:1,000 (IF); anti-Arfaptin 1:10,000 (WB); anti-FAPP2 1:3,000 (WB); anti-GFP 1:10,000 (WB) and anti-GST 1:1,000 (IF), 1:10,000 (WB) polyclonal antibodies; recombinant GST–PI(4)KIIIβ fragments and PI(4)KIIIβ–CFP$^{wt}$ complementary DNA, M. A. De Matteis (Tigem); anti-giantin monoclonal antibody 1:1,000 (IF), H. P. Hauri (Basel University); PAK Flag-AID, E. Manser (Institute of Molecular and Cell Biology, Singapore); IPA-3 inhibitor, J. Chernoff (Fox Chase Cancer Center); VSVG–GFP, VSVG–CFP and VSVG–KDELR cDNAs, J. Lippincott-Schwartz (National Institutes of Health); p75–GFP cDNA, E. Rodriguez-Boulan (Weill Cornell Medical College), and VSV, K. Simons (Max Planck Institute). The rabbit polyclonal anti-14-3-3γ antibody (1:100 (IF); 1:2,000 (WB)) was raised against GST–14-3-3γ. Commercially available antibodies used: anti-14-3-3γ (C-16) (IP), anti-14-3-3ε (T-16) (IP), anti-PKCμ (C-20) 1:500 (WB), anti-PAK (C-19 and N-20) 1:50 (IF), 1:100 (WB) and anti-Myc 1:100 (IF), 1:500 (WB) (Santa Cruz Biotechnology) polyclonal antibodies; anti-14-3-3τ (IP; 1:50 (IF), 1:5,000 (WB)), anti-14-3-3σ (IP; 1:500 (WB)) and anti-GFP 1:500 (IF), 1:1,000 (WB) (Abcam) monoclonal antibodies; M2-anti-Flag monoclonal 1:500 (IF), 1:5,000 (WB), P5D4 Cy3-conjugated anti-VSVG 1:400 (IF), 1:20,000 (WB) and anti-phospho-PAK1/2/3 (pThr-423) 1:100 (IF) (Sigma) antibodies; anti-14-3-3γ monoclonal antibody 1:10,000 (WB) (Upstate Biotechnology); anti-14-3-3β/ζ monoclonal antibody (IP; 1:1,000 (WB)) (StressGen Biotechnologies Corp); mouse anti-GAPDH 1:50,000 (WB) and anti-TGN46 1:1,000 (IF) antibodies (AbD Serotec); 1C8 anti-phosphoserine monoclonal IgM 1:1,000 (WB) (Biomol); anti-14-3-3ε 1:500 (WB) and anti-14-3-3η (IP; 1:1,000 (WB)) (Cell Signaling) polyclonal antibodies; anti-PAK3 monoclonal antibody 4 μg ml$^{-1}$ (IF) (Abnova); anti-ARF1 (1D9) monoclonal antibody 1:75 (IF) (ABR) and anti-CtBP1 monoclonal antibody 1:50 (electron microscopy) (BD Transduction Laboratories). The anti-pentahistidine monoclonal antibody 1:1,000 (WB), Alexa 488 and 546 conjugated secondary antibodies, TRICH-labelled dextran and FITC-labelled dextran were from Molecular Probes. Anti-IgM was from Calbiochem. Human 14-3-3γ cDNA was from MRC Geneservice (for subcloning and mutation, see Supplementary Table S1). Lipofectamine 2000 was from Invitrogen; TransIT-LT1 (MIR 2300) from Mirus; calyculin A from Calbiochem; protease inhibitors (Complete Mini EDTA-free) from Roche; and tannic acid and BFA from Fluka. His–BARS, His–BARS-NBD, His–BARS-SBD and GST–BARS were prepared as described[24]; the same procedures were used for GST–14-3-3γ, GST–14-3-3γ$^{Q13QR}$ and His–14-3-3γ (with 1 mM isospropyl-β-D-1-thiogalactopyranoside induction for 2 h). siRNAs were from Dharmacon (Supplementary Table S2).

**Rat-brain cytosol.** Rat-brain cytosol was prepared as described[66], with modifications. Rat brains were isolated, washed in buffer A (50 mM HEPES at pH 7.4, 320 mM sucrose) and transferred to ice-cold buffer B (50 mM HEPES at pH 8.0, 250 mM sucrose, 500 mM KCl, 1 mM dithiothreitol (DTT), 2 mM EGTA, protease inhibitors) and homogenized in 12 ml (Ultraturrax; Janke & Kunke). The homogenate was centrifuged (5,000*g*, 30 min, 4 °C), and the supernatant was ultracentrifuged (150,000*g*, 90 min, 4 °C). The supernatant was dialysed (4 h, 4 °C) against dialysis buffer (50 mM HEPES at pH 8.0, 50 mM KCl, 1 mM DTT) (sample:dialysis buffer, 1:140). Precipitate formed during dialysis was removed by centrifugation (150,000*g*, 60 min, 4 °C). The supernatant was aliquoted, frozen in liquid nitrogen and stored at −80 °C.

**Rat-liver Golgi membranes.** Golgi membranes were obtained as described[67], with modifications. Briefly, 30 mg rat-liver tissue minced in 140 ml of 0.5 M sucrose was homogenized (Ultraturrax). The homogenate was centrifuged (600*g*, 10 min, 4 °C). The supernatant (~120 ml) was split into 20 ml aliquots that were layered onto 18 ml 1.3 M sucrose cushions and centrifuged (105,000*g*, 60 min, 4 °C; swing-out rotor). The 0.5/1.3 M sucrose interface (~2.5 ml/tube) was collected (~16 ml total), and the sucrose concentration adjusted to 1.1 M with 2.3 M sucrose (Bausch and Lomb refractometer); the volume was brought to 18 ml with 1.1 M sucrose. The suspension was split into two and layered onto sucrose gradients (7.5 ml 1.4 M, 7.5 ml 1.3 M and 7.5 ml 1.25 M sucrose, from the bottom of tubes for the swing-out rotor) and covered with 6.5 ml of 0.5 M sucrose. After centrifugation (105,000*g*, 90 min, 4 °C), the Golgi-enriched fraction was collected at the 0.5/1.1 M sucrose interface, aliquoted, frozen in liquid nitrogen and stored at −80 °C.

To solubilize Golgi membranes used in pulldown assays, 4 mg Golgi membrane protein (800 μl) was resuspended at threefold dilution in 10 mM HEPES at pH 8.0, 100 mM KCl, with protease and phosphatase inhibitors (1 μM sodium orthovanadate, 20 mM β-glycerophosphate, 10 mM NaF) and centrifuged twice (20,000*g*, 10 min, 4 °C). The final pellet was solubilized (30 min, 4 °C) in 400 μl 20 mM HEPES at pH 8.0, 100 mM KCl, 1% Triton X-100, 2 mM EDTA, protease and phosphatase inhibitors. This suspension was diluted 1:1 with water, and centrifuged (2,000*g*, 10 min, 4 °C); the supernatant represented the 'solubilized Golgi membranes'.

**Immunoprecipitation.** BARS-IgG and preimmune-IgG matrices were obtained by crosslinking 1 ml protein A Sepharose (Amersham) to 500 μg affinity-purified p50-2 rabbit anti-BARS-IgG and rabbit preimmune-IgG, respectively, as described[65]. To isolate BARS-interacting proteins, 160 mg rat-brain cytosol protein was brought to 0.2% (w/v) Triton X-100 (final concentration), supplemented with protease inhibitors. This was mixed with 1 ml BARS-IgG matrix or preimmune-IgG matrix, both previously equilibrated in HKT buffer (50 mM HEPES at pH 8.0, 100 mM KCl, 0.2% Triton X-100, protease inhibitors), and incubated on a shaker (3 h, 4 °C). The matrices were transferred into two chromatographic columns. The flow-through from each was collected and each column was washed twice with 10 ml HKT buffer, then twice with HK buffer (HKT buffer without Triton X-100). In the meantime, 1.5 ml tubes filled with 1.2 mg ml$^{-1}$ BSA in PBS were incubated for 30 min at room temperature. The BSA was removed and tubes were washed once with HK buffer. Finally, the proteins were eluted from the columns with 0.1 M glycine at pH 3.0, collecting 0.5 ml fractions in the BSA-pretreated tubes, to reduce loss of protein by attachment onto plastic. The third fractions contained most of the eluted proteins; these were separated using 4%–15% gradient SDS–PAGE, and revealed by silver staining. Bands for mass spectrometry analysis were selected by comparing proteins eluted from the anti-BARS-IgG matrix with proteins eluted from the control-IgG matrix. The bands were excised from the gel, trypsin digested, run on matrix-assisted laser desorption/ionization–time of flight and then electrospray ionization–tandem mass spectrometry was carried out at the Molecular Structure Facility, University of California, USA. Matrix-assisted laser desorption/ionization–time of flight, peptide mass mapping and *de novo* sequence data identified $P_7$ as 14-3-3γ (Fig. 1a). The subsequent characterization and validation of 14-3-3γ as a major BARS interactor (see main text) used different biochemical and functional approaches.

For immuno-affinity purification of BARS-interacting proteins, COS7 cells were washed with PBS, harvested by trypsinization, pelleted and washed three times in PBS. Whole-cell extracts were obtained by resuspending cell pellets in lysis buffer (20 mM Tris at pH 7.4, 150 mM KCl, 5 mM $MgCl_2$, 1 mM DTT, 5 mM EGTA) supplemented with 1% Triton X-100 and protease inhibitors, on a shaker (30 min, 4 °C). The lysates were centrifuged (13,000*g*, 10 min, 4 °C) and brought to 0.2% (w/v) Triton X-100 (final concentration). Thirty-two milligrammes of lysate protein was split into two, with 16 mg mixed with 100 μl BARS-IgG matrix or preimmune-IgG matrix (volume corresponding to 50 μg crosslinked IgGs) previously equilibrated in lysis buffer with 0.2% Triton X-100 (two washes), and incubated (3 h, 4 °C, shaking). The suspensions were centrifuged (700*g*, 5 min) and supernatants recovered (that is, flow-through). The matrices were washed four times with lysis buffer with 0.2% Triton X-100, and twice with lysis buffer without Triton X-100, centrifuging as before. The proteins were eluted with three volumes of 0.1 M glycine at pH 3.0, added to the matrices three times, with each incubated for 10 min (4 °C, shaking). Eluted proteins were recovered after centrifugation (700*g*, 5 min) and neutral pH restored by adding 1 M Tris at pH 11.0. Thirty per cent of the precipitated protein was separated on 4%–15% gradient SDS–PAGE, transferred onto nitrocellulose (Millipore) and subjected to western blotting.

The immunoprecipitation from COS7 cell lysates pretreated with calyculin A was carried out according to the above procedures, except that 50 nM calyculin A in complete medium was added (10 min, 37 °C) before cell lysis. The same lysis buffer with 0.2% Triton X-100 and phosphatase inhibitors (20 mM β-glycerophosphate, 1 μM sodium orthovanadate, 10 mM NaF) was used to wash the non-crosslinked IgG-bound matrices used, and the co-immunoprecipitated proteins were eluted by boiling (10 min) in 100 μl Laemmli buffer, and separated on 8% SDS–PAGE gels, before transfer onto nitrocellulose.

Immunoprecipitation to test 14-3-3-isoform-specific interactions between 14-3-3γ and BARS was as follows. Five milligrammes of rat-brain cytosol protein/sample was brought to 0.2% (w/v) Triton X-100 (final concentration) and supplemented with protease inhibitors. Ten microgrammes of the specific antibody was added to samples (2 h, 4 °C, shaking). For each monoclonal antibody, 50 μl protein G Sepharose beads/sample (Sigma; or protein A Sepharose for polyclonal antibodies) were added. Samples were incubated (1 h, 4 °C, shaking), and immune complexes collected by centrifugation (700*g*, 5 min). The beads were washed thrice with HKT buffer (as above) and twice with HK buffer, and centrifuged as before. Immunoprecipitated proteins were eluted by boiling (10 min) in 100 μl Laemmli buffer, separated on 8% SDS–PAGE gels, and transferred onto nitrocellulose.

Immunoprecipitation to characterize 14-3-3γ dimerization determinants was as described[68], with modifications. COS7 cells in 10 cm plates were transiently transfected with plasmids using 36 μl TransIT-LT1 and 6 μg of each DNA per plate. Twenty-four hours after transfection, cells were washed with PBS, harvested by trypsinization, pelleted and washed thrice with PBS. Whole-cell extracts were obtained by resuspending and solubilizing the cell pellets in TNN buffer (10 mM Tris

DOI: 10.1038/ncb2445

at pH 7.5, 150 mM NaCl, 1% NP-40, protease inhibitors and phosphatase inhibitors; 2 mM sodium orthovanadate, 100 nM okadaic acid) (15 min, 4 °C, shaking). Lysates were centrifuged (13,000*g*, 20 min). Seven hundred microgrammes of lysate protein were incubated overnight with 2.5 µg mouse anti-Flag antibody, and then 30 µl protein G Sepharose beads were added for another hour. After three washes with TNN buffer and two with TNN buffer without NP-40, bound protein was eluted by boiling (10 min) in 100 µl Laemmli buffer. Immunoprecipitated proteins and 30 µg total cell lysates were separated on 12% SDS–PAGE gels and transferred onto nitrocellulose. As Flag-tagged and Myc-tagged 14-3-3 proteins are almost the same size, for each immunoprecipitation, two gels were loaded with half of each eluate.

**GST pulldown.** Equimolar amounts of GST–PI(4)KIIIβ (120 µg), GST–14-3-3γ (55 µg) or GST (30 µg) were coupled to glutathione Sepharose beads (Amersham), and incubated with 50 µg His–BARS or 5 mg rat-brain cytosol protein, in 20 mM Tris at pH 8.0, 100 mM KCl, 1 mM EDTA, 0.2% Triton X-100 and protease inhibitors (2 h, 4 °C, shaking). Following extensive washing of beads, interacting proteins were eluted with 100 mM Tris at pH 8.0, 20 mM reduced glutathione, 5 mM DTT; relevant fractions were examined by SDS–PAGE and western blotting.

**Histidine pulldown.** Histidine pulldown assays were carried out as described[38], with modifications. Six microgrammes immobilized recombinant His–BARS was added to 50 µl Ni-NTA agarose beads (Amersham) and incubated with 50 µg purified GST–14-3-3$\gamma^{wt}$, or GST–14-3-3$\gamma^{Q13QR}$, or GST in incubation buffer (50 mM $NaH_2PO_4$, 150 mM NaCl, 20 mM imidazole at pH 8.0, 0.2% Triton X-100, protease inhibitors; 2 h, 4 °C, rotating wheel). The beads were washed thrice with incubation buffer by centrifugation (700*g*, 5 min) and then mixed with 5 mg rat-brain cytosol (supplemented with protease inhibitors and 0.2% w/v Triton X-100) for 2 h. Beads were washed once with 10 volumes of incubation buffer, and twice with incubation buffer without Triton X-100, and centrifuged as before. Proteins were eluted with 300 µl elution buffer (50 mM $NaH_2PO_4$, 150 mM NaCl, 250 mM imidazole, pH 8.0, protease inhibitors), centrifuged (700*g*, 5 min), and about one-third examined by 8% SDS–PAGE and western blotting.

**Transfection with siRNAs.** COS7 cells were transfected with 100 nM Smart Pool of indicated siRNA sequences or non-targeting siRNA (except for *PAK* siRNAs, where 150 nM Smart Pool was used), for 48 h using Lipofectamine 2000, according to manufacturer's instructions. The efficiency of interference was assessed by western blotting. Alternatively, COS7 cells were transfected with siRNAs (as above) in combination with VSVG–GFP, VSVG–CFP or p75–GFP, and after 48 h they were subjected to the TGN-exit assay[17].

For rescue experiments, COS7 cells were transfected with 100 nM siRNA 14-3-3γ/D-008844-02 (5′-GCGAGCAACUGGUGCAGAAUU-3′, Dharmacon) for 24 h, and transfected for a further 24 h (TransIT-LT1 transfectant) with Flag–14-3-3$\gamma^{wt}$ or Flag–14-3-3$\gamma^{Q13QR}$ (both encode an siRNA-resistant silent mutation) before infection with VSV for the TGN-exit assay. Briefly, for 14-3-3$\gamma^{Q13QR}$, the residues involved in dimerization of mammalian 14-3-3γ (Leu-13, Ala-14, Glu-15; were identified by homology with equivalent residues shown to mediate dimerization of *Drosophila* 14-3-3 ζ (ref. 69) and according to a previous report[68]), and mutated to Gln13, Gln14 and Arg15.

**TGN-exit assay, microinjection and light microscopy.** The TGN-exit assay of p75, VSVG–GFP/CFP-transfected and VSV-infected COS7 cells and microinjection were carried out as reported[17].

To visualize VSVG-containing carriers, 0.5% tannic acid was added to VSVG-expressing cells before release of 20 °C temperature-block during the TGN-exit assay. The cells were shifted to 32 °C, fixed, labelled with the p5D4 anti-VSVG antibody and analysed by confocal microscopy.

To quantify VSVG-containing carriers, cells were labelled with the P5D4 anti-VSVG antibody and an anti-TGN46 antibody, and images of the confocal plane closest to the base of the cell (where most carriers are located in flattened cells) were acquired. The number of fluorescent spots (0.5–2.0 µm) co-stained by the two antibodies (at least 80% of VSVG-containing carriers) was then counted. PGC quantification indicates the mean number per cell from at least 100 cells per time per experiment analysed.

**Wide-field microscopy.** COS7 cells were plated on MatTEK-coverslip-bottomed dishes (MatTEK Corporation), transfected after 24 h with VSVG–CFP and either BARS$^{wt}$–YFP or BARS$^{S147A}$–YFP mutant (TransIT-LT1 reagent; Mirus) for 4–6 h, left overnight at 40 °C and then incubated (3 h, 20 °C) with cycloheximide. Cells were then shifted to 32 °C (with cycloheximide), and followed by fast videomicroscopy[70] (500 ms per frame), with a 63 × 1.4 NA objective and IX70 microscope (Olympus) equipped with a TILL-Photonics-imagine system. A monochromator was used to sequentially excite CFP (430 nm) and YFP (514 nm). For detection, narrow-band filters from Chroma were used (ET 480/40 nm for CFP, ET 535/30 nm for YFP) to ensure best separation of fluorescent proteins. Under these conditions, the lack of bleed-through of the CFP and YFP channels was checked and ensured.

**Ion-exchange chromatography.** MonoQ and MonoS chromatography were as described[36], with modifications. Thirty 10 cm dishes of COS7 cells pretreated with 50 nM calyculin A (complete medium, 10 min, 37 °C) were lysed. Cells were washed with PBS, harvested by trypsinization, pelleted and washed thrice with PBS. Whole-cell extracts were obtained by resuspending and solubilizing cell pellets (30 min, 4 °C) in lysis buffer (25 mM Tris at pH 8.0, 5 mM $MgCl_2$, 1 mM DTT, 5 mM EGTA, 1% Triton X-100, protease and phosphatase inhibitors). Lysates were centrifuged twice (10,000*g*, 10 min), and brought to 0.2% (w/v) Triton X-100 final concentration. Forty milligrammes of total-lysate protein (2 mg ml$^{-1}$) were applied to a MonoQ column (HR5/5 Pharmacia LKB) equilibrated with lysis buffer with 0.2% Triton X-100 (4 °C; flow rate, 1 ml min$^{-1}$); 1 ml fractions were collected. After washing with lysis buffer, proteins were eluted on a fast protein liquid chromatography system, with a 30 ml (0.0–0.5 M) NaCl gradient, and 25 µl of the collected fractions were separated on 10% SDS–PAGE gels and analysed by western blotting. Fractions 53–55 were combined, dialysed twice against 1,000 volume dialysis buffer (50 mM MES at pH 6.5, 5 mM $MgCl_2$, 1 mM DTT, 5 mM EGTA, 0.2% Triton X-100, protease and phosphatase inhibitors). This pool was then applied to a MonoS column (HR5/5 Pharmacia-LKB) equilibrated with dialysis buffer, and eluted with a 30 ml (0.0–0.5 M) NaCl gradient, with 1 ml fractions collected.

Seventy-five microlitres of each fraction was separated on 10% SDS–PAGE and analysed by western blotting. Nine hundred microlitres of fractions 27–34 were adjusted to 300 mM NaCl (including 1 mM DTT, protease and phosphatase inhibitors) and immunoprecipitated with a polyclonal anti-BARS antibody. Bound protein was added to Laemmli buffer, separated on 10% SDS–PAGE gels, and analysed by western blotting.

**apFRET and FLIM measurements.** Acceptor photobleaching experiments were carried out with a Zeiss LSM 510 meta, Zeiss LSM 710 or Leica SP2 confocal microscope, as follows: for CFP (donor) fluorescence detection, excitation at 405 nm (or 458 nm for Leica SP2) and fluorescence detected at 470–490 nm. For YFP bleaching, a 514 nm argon laser was used. apFRET was measured by increase in CFP fluorescence intensity before ($I_{DA}$) and after ($I_D$) YFP photobleaching. To ensure reproducibility and reliability of CFP fluorescence measurements in the absence of acceptor ($I_D$), YFP was photobleached to 10% of its initial fluorescence. The FRET efficiency was calculated as $E = (I_D - I_{DA})/I_D$. Lifetime imaging was carried out with a Leica TCS-SMD-FLIM (single-photon) confocal microscope, with a 20 MHz frequency-modulated 405 nm excitation laser, 450–490 nm fluorescence detection, 1.3 µm optical slice thickness, 40×/1.2 NA objective and 0.2 µm (0.04 µm$^2$) *x*–*y* pixel sampling of 1,000 detected photons per pixel (gate based on brightest pixel). Lifetime calculation was carried out in specific regions of interest, corresponding to the Golgi area. To evaluate lifetime distribution on a single pixel basis with the best statistical significance, a threshold was applied to limit analysis to pixels with more than 500 total collected photons. Lifetime was determined per single thresholded pixel, and used to build histograms of lifetime versus pixel percentage (pixel percentage calculated with reference to total pixels of region of interest). For lifetimes and relative amplitudes, the acquired fluorescence decay was deconvolved with the instrument response function, and fitted by a Levenberg–Marquardt least-square algorithm, using the Leica Application Suite Advanced Fluorescence software. With a distribution of lifetimes, amplitude-averaged lifetime values were used, calculated as $\tau = \sum(\alpha_i\tau_i)/\sum\alpha_i$ where $\alpha_i$ is the amplitude of each lifetime, $\tau_i$. FRET efficiency ($E$) was calculated as $E = 1 - \tau_{DA}/\tau_D$, where D indicates donor fluorescence lifetime in the absence of an acceptor, and DA indicates this in the presence of an acceptor.

**COPI transport and macropinocytosis.** COPI transport and macropinocytosis assays were carried out in COS7 cells and A431 cells, respectively, as described[39,46].

**Statistical analysis.** Two-tailed Student *t*-tests were applied to the data. $^{*}P < 0.05$, $^{**}P < 0.01$, $^{***}P < 0.005$.


65. Harlow, E. & Lane, D. *Antibodies: A Laboratory Manual* (CSH Press, 1988).
66. Malhotra, V., Serafini, T., Orci, L., Shepherd, J. C. & Rothman, J. E. Purification of a novel class of coated vesicles mediating biosynthetic protein transport through the Golgi stack. *Cell* **58,** 329–336 (1989).
67. Leelavathi, D. E., Estes, L. V., Feingold, D. S. & Lombardi, B. Isolation of a Golgi rich fraction from rat liver. *BBA* **211,** 124–138 (1970).
68. Verdoodt, B., Benzinger, A., Popowicz, G. M., Holak, T. A. & Hermeking, H. Characterization of 14-3-3σ dimerization determinants: requirement of homodimerization for inhibition of cell proliferation. *Cell Cycle* **5,** 2920–2926 (2006).
69. Zhou, Y., Reddy, S., Murrey, H., Fei, H. & Levitan, I. B. Monomeric 14-3-3 protein is sufficient to modulate the activity of the *Drosophila* slowpoke calcium-dependent potassium channel. *J. Biol. Chem.* **278,** 10073–10080 (2003).
70. Keller, P., Toomre, D., Diaz, E., White, J. & Simons, K. Multicolour imaging of post-Golgi sorting and trafficking in live cells. *Nat. Cell Biol.* **3,** 140–149 (2001).

DOI: 10.1038/ncb2445

nature cell biology

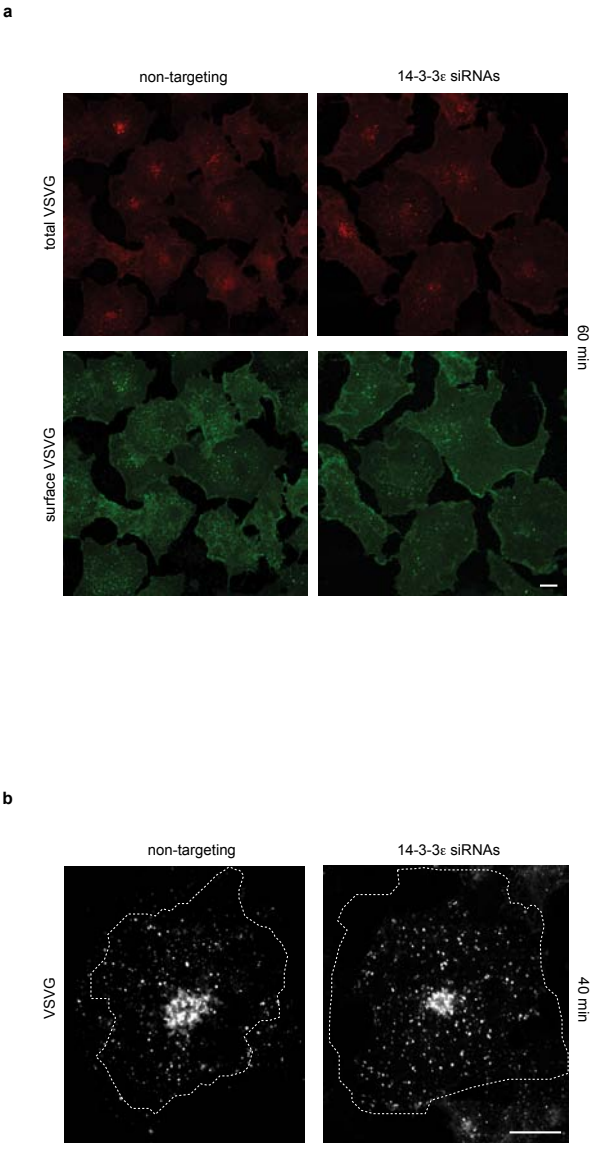


**Figure S1** 14-3-3ε depletion does not reduce the formation of VSVG-positive post-Golgi-carriers. COS7 cells were transfected with non-targeting or 14-3-3ε siRNAs, VSV infected, and subjected to the TGN-exit assay without (**a**) or with 0.5% tannic acid **(b)**. Representative confocal images of cells fixed 60 min (**a**) or 40 min (**b**) after the 32°C temperature-block release. **(a)** Total VSVG was stained after permeabilisation (red, P5D4 anti-VSVG antibody). Surface VSVG was stained without permeabilisation (green, lumenal domain anti-VSVG antibody). **(b)** VSVG-positive post-Golgi-carriers were stained after permeabilisation with P5D4 anti-VSVG antibody (white). Dotted lines: cell borders. Scale bars, 10 μm.

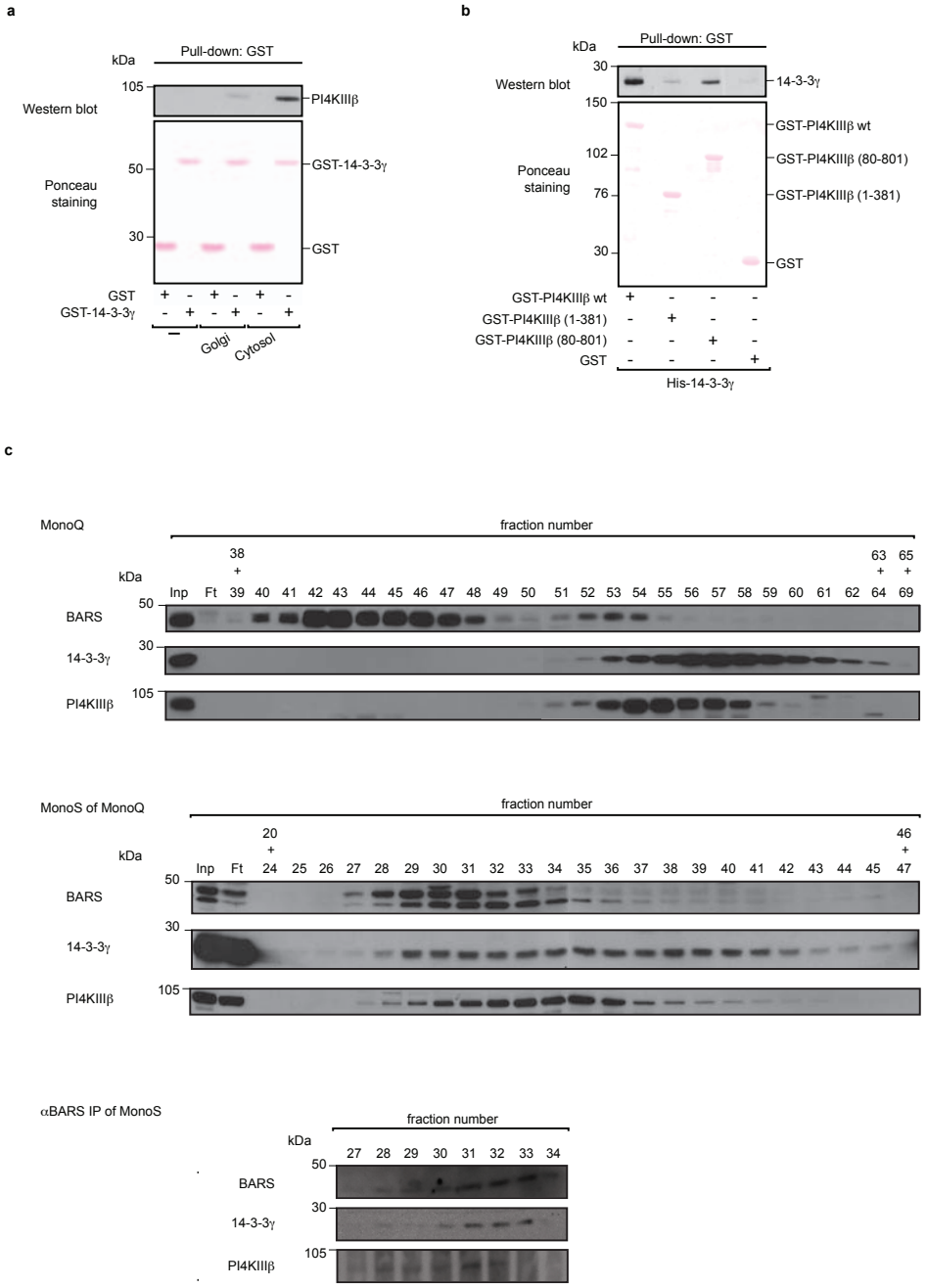


**Figure S2** 14-3-3γ and PI4KIIIβ directly interact and co-elute with BARS on ion-exchange chromatography. GST pull-down assays were performed incubating: **(a)** Buffer alone (-), solubilised Leelavathi Golgi membranes (Golgi; 2 mg) or rat-brain cytosol (Cytosol; 5 mg), with equimolar amounts of GST-14-3-3γ or GST; **(b)** Recombinant His-14-3-3γ (3 μg) with equimolar amounts of GST-PI4KIIIβ wild-type (12 μg), GST-PI4KIIIβ (1-381 aa; 7 μg), GST-PI4KIIIβ (80-801 aa; 11 μg) or GST (3 μg). **(a, b)** The bound proteins were eluted and analysed by Western blotting (top) using PI4KIIIβ (a) and 14-3-3γ (b) polyclonal antibodies. The GST fusion proteins were visualised by Ponceau-S staining (bottom). **(c)** BARS, 14-3-3γ and PI4KIIIβ co-elution on ion-exchange chromatography. COS7 cell lysates were applied to a MonoQ ion-exchange chromatography column and eluted with a NaCl gradient. Aliquots of each fraction were analysed by Western blotting (antibodies as indicated; top). BARS, 14-3-3γ and PI4KIIIβ showed fairly broad elution profiles that overlapped only moderately, probably as these proteins can participate in different complexes. The 'overlap' fractions (MonoQ, 53-55) were combined and applied to a MonoS ion-exchange chromatography column. The MonoS was eluted with a NaCl gradient, and aliquots of each fraction were analysed by Western blotting (antibodies as indicated; middle). Despite very different isoelectric points, BARS, 14-3-3γ and PI4KIIIβ co-elute (MonoS, 27-34). Aliquots of fractions 27 to 34 were immunoprecipitated using an anti-BARS polyclonal antibody. The BARS-immunoprecipitates were separated on SDS-PAGE, transferred to nitrocellulose, and probed with antibodies as indicated (bottom). BARS, 14-3-3γ and PI4KIIIβ are recovered as a robust complex by co-immunoprecipitation after these two different ion-exchange columns. Molecular weight standards (kDa) indicated on left of each panel.

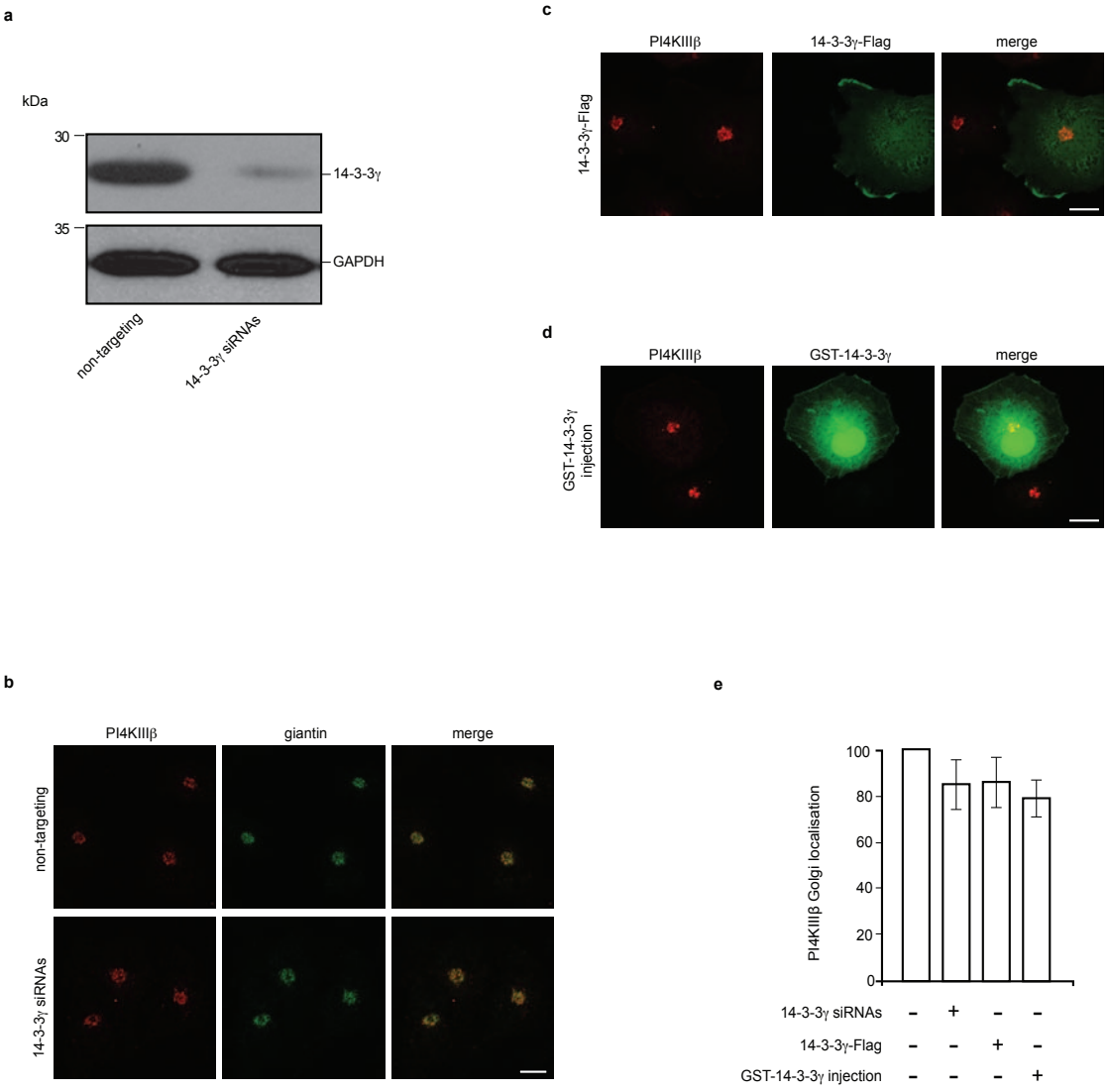


**Figure S3** PI4KIIIβ localisation at the Golgi complex is 14-3-3γ independent. (**a**) Representative immunoblotting of COS7 cells treated with non-targeting siRNAs or with 14-3-3γ-directed siRNAs and processed for immunoblotting of 14-3-3γ knock-down, as revealed with anti-14-3-3γ and anti-GAPDH antibodies. **(b)** Representative images of cells from **a**, labelled with an anti-PI4KIIIβ polyclonal antibody (red) and with an anti-giantin monoclonal antibody (green, Golgi marker) to follow cells positive for PI4KIIIβ in the Golgi area. **(c)** Representative images of COS7 cells transfected with Flag-tagged 14-3-3γ for 24 h and labelled with an anti-PI4KIIIβ polyclonal antibody (red) and with an anti-Flag monoclonal antibody (green). **(d)** Representative images of COS7 cells injected with recombinant GST-14-3-3γ (1-2 mg $ml^{-1}$) together with fluorescent dextran as injection marker (GST-14-3-3γ injection; green), 15-18 h before fixing, and labelled with an anti-PI4KIIIβ polyclonal antibody (red). The GST injection does not affect PI4KIIIβ localisation at the Golgi complex (data not shown). (**e**) Quantification of PI4KIIIβ Golgi localisation as described in **b**-**d**. Data are means ±s.d. of three independent experiments. (**b, c, d**) Scale bars, 10 μm.

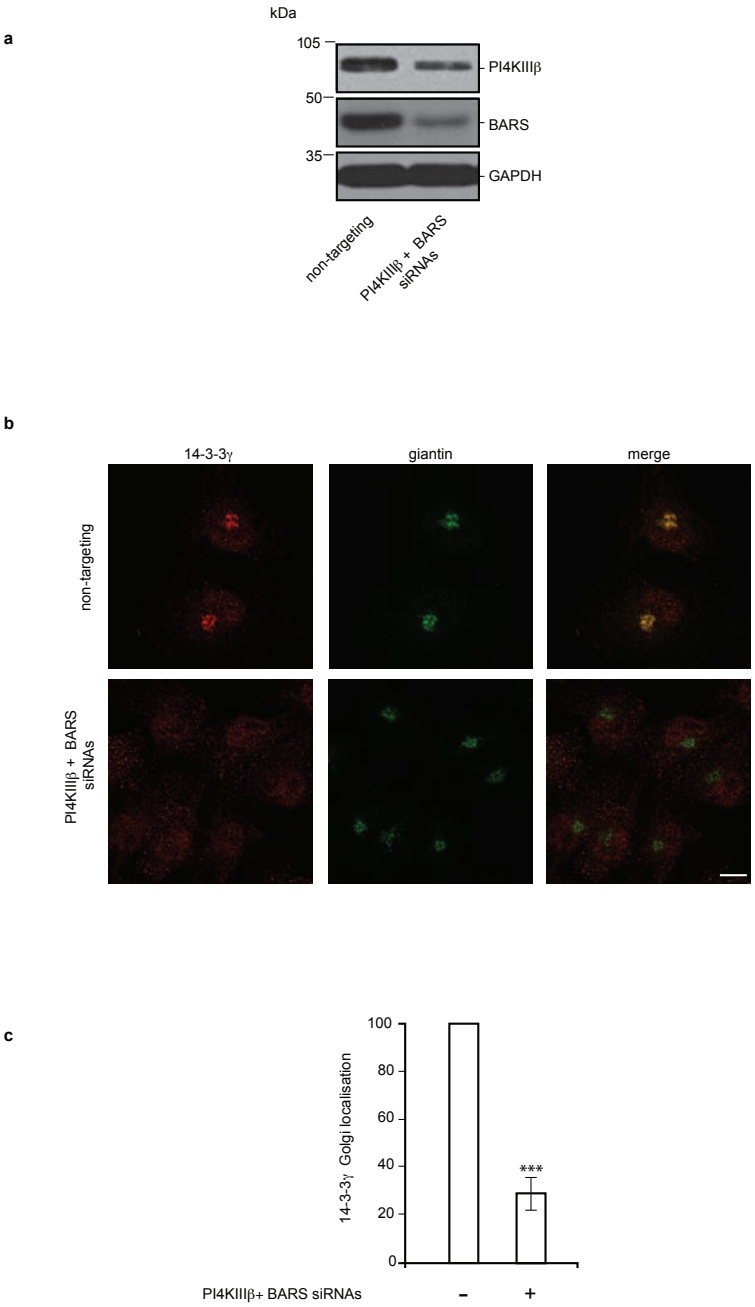


**Figure S4** Depletion of both BARS and PI4KIIIβ proteins caused a marked redistribution of 14-3-3γ from the Golgi complex to the cytosol. (**a**) Representative imunoblotting of COS7 cells treated with non-targeting siRNAs or PI4KIIIβ-directed plus BARS-directed siRNAs and processed for immunoblotting with anti-PI4KIIIβ, anti-BARS and anti-GAPDH antibodies, to reveal PI4KIIIβ and BARS knock-down. **(b)** Representative images of cells from **a**, labelled with an anti-14-3-3γ polyclonal antibody (red) and an anti-giantin monoclonal antibody (green, Golgi marker), to identify cells positive for 14-3-3γ in the Golgi area. Scale bar, 10 μm. (**c**) Quantification of 14-3-3γ Golgi localisation as described in **b**. Data are means ±s.d. of three independent experiments. ***P <0.005 (Student's *t*-test).

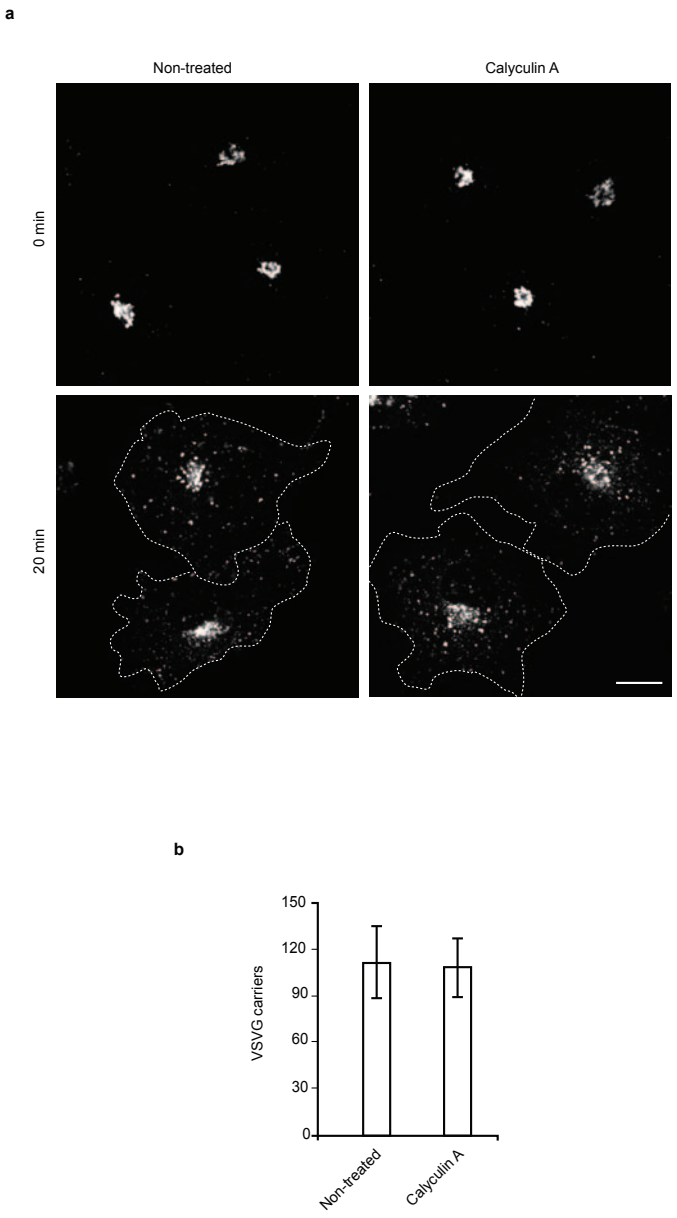


**Figure S5** Calyculin A treatment does not affect VSVG-containing post-Golgi-carrier formation. **(a)** Representative confocal images of VSV-infected COS7 cells subjected to the TGN-exit assay, with 0.5% tannic acid. The cells were fixed after 3 h incubation at 20 °C (0 min), or after 20 min of incubation at 32 °C (20 min), and stained with the P5D4 anti-VSVG antibody, to identify VSVG-positive PGCs. During the incubation at 32 °C, the cells were either left untreated (Non-treated) or treated with 50 μM calyculin A. Treatments with calyculin A longer than 30 min caused toxic effects. Dotted lines: cell borders. Scale bar, 10 μm. **(b)** Quantification of VSVG-containing PGCs in COS7 cells treated as in **a**, with PGC formation per cell counted after 20 min of 32 °C temperature-block release (see Methods). Data are means ±s.d. of three independent experiments.

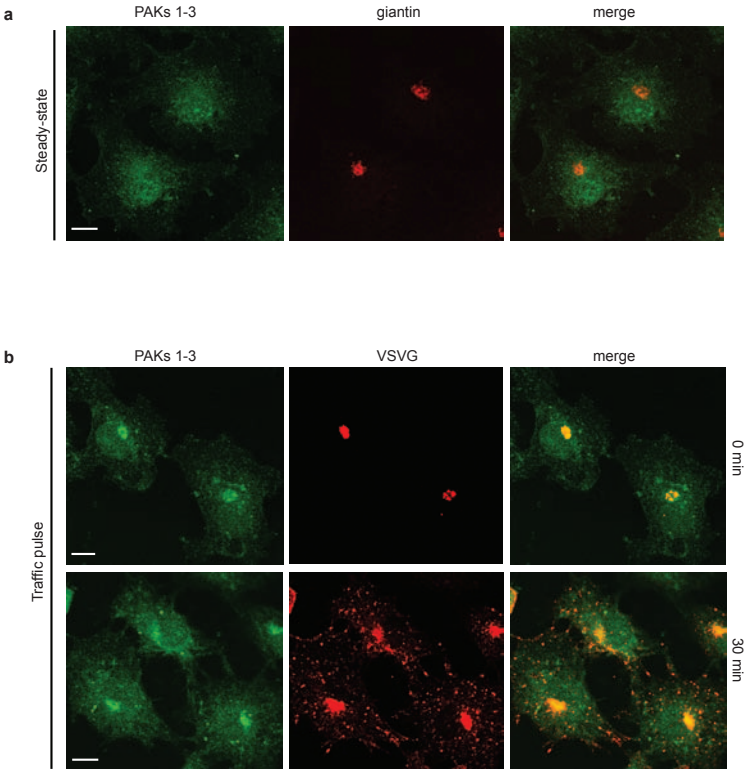


**Figure S6** Localisation of PAKs 1-3 in COS7 cells. **(a)** Representative confocal images of non-transfected COS7 cells at steady-state, labelled with an anti-PAKs 1-3 polyclonal antibody (green, endogenous PAKs 1-3) and with an anti-giantin monoclonal antibody (red, Golgi marker). **(b)** A VSVG traffic pulse induces PAK recruitment onto the Golgi. COS7 cells were VSV-infected and subjected to the VSVG TGN-exit assay. The cells were fixed after 3 h at 20 °C (0 min), or after 30 min at 32 °C (30 min), and stained with an anti-PAKs 1-3 polyclonal antibody (green) and with the P5D4 anti-VSVG antibody (red). Scale bars, 10 μm.

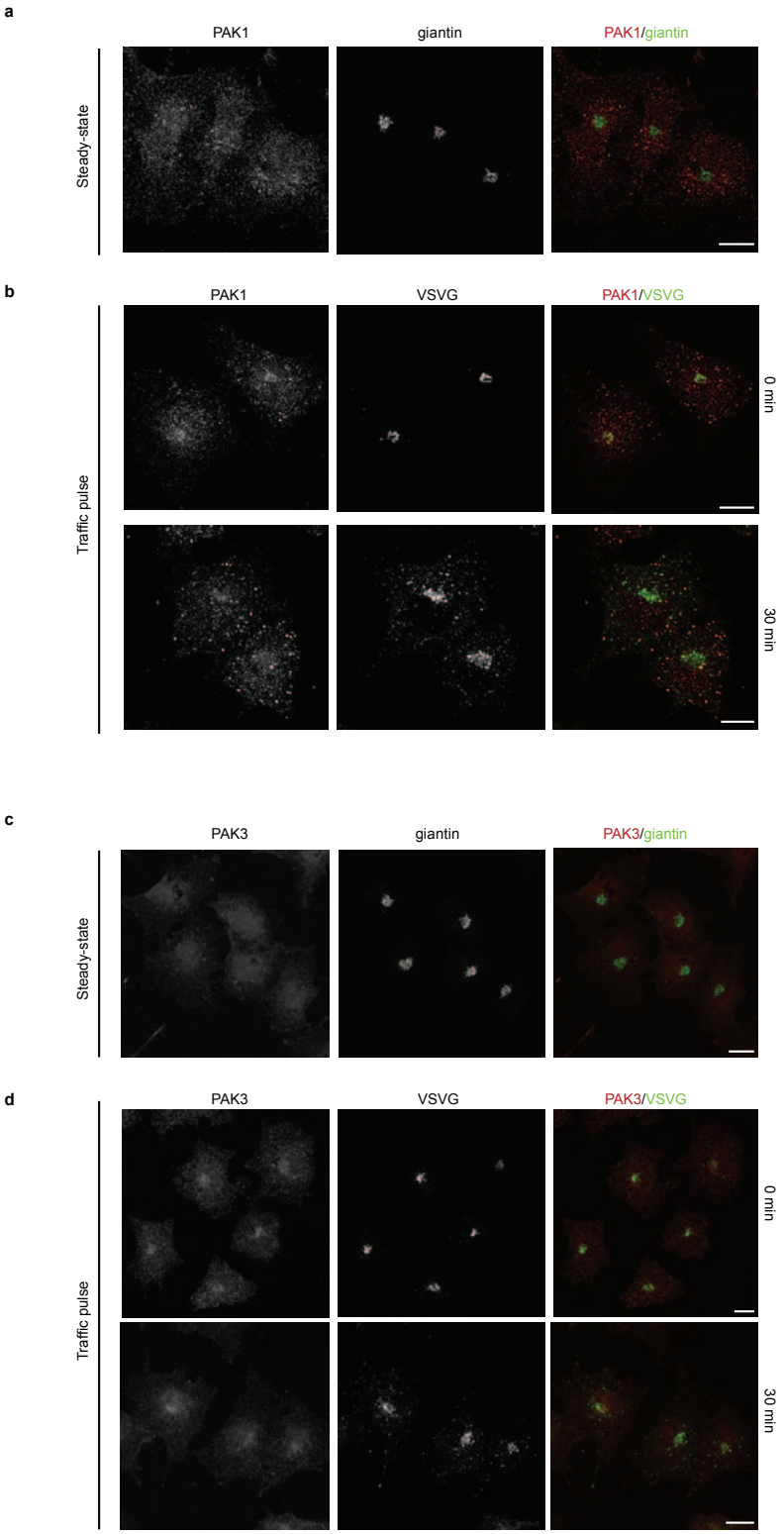


**Figure S7** Localisation of PAK1 and PAK3 in COS7 cells. Representative confocal images of COS7 cells at steady-state (**a, c**) or VSV-infected and subjected to the VSVG TGN-exit assay (Traffic pulse; **b, d**). The cells were fixed and labelled with the N-20 anti-PAK1 polyclonal antibody (endogenous PAK1; **a, b**) or an anti-PAK3 monoclonal antibody (endogenous PAK3; **c, d**), plus an anti-giantin antibody (Golgi marker; **a, c**) or the P5D4 anti-VSVG antibody after 3 h at 20 °C (0 min) or after 30 min at 32 °C (30 min) (**b, d**). PAK1 (red, **a, b**) and PAK3 (red, **c, d**) and giantin (green, **a, c**) and VSVG (green, **b, d**) are shown in the merge panels. Scale bars, 10 μm.

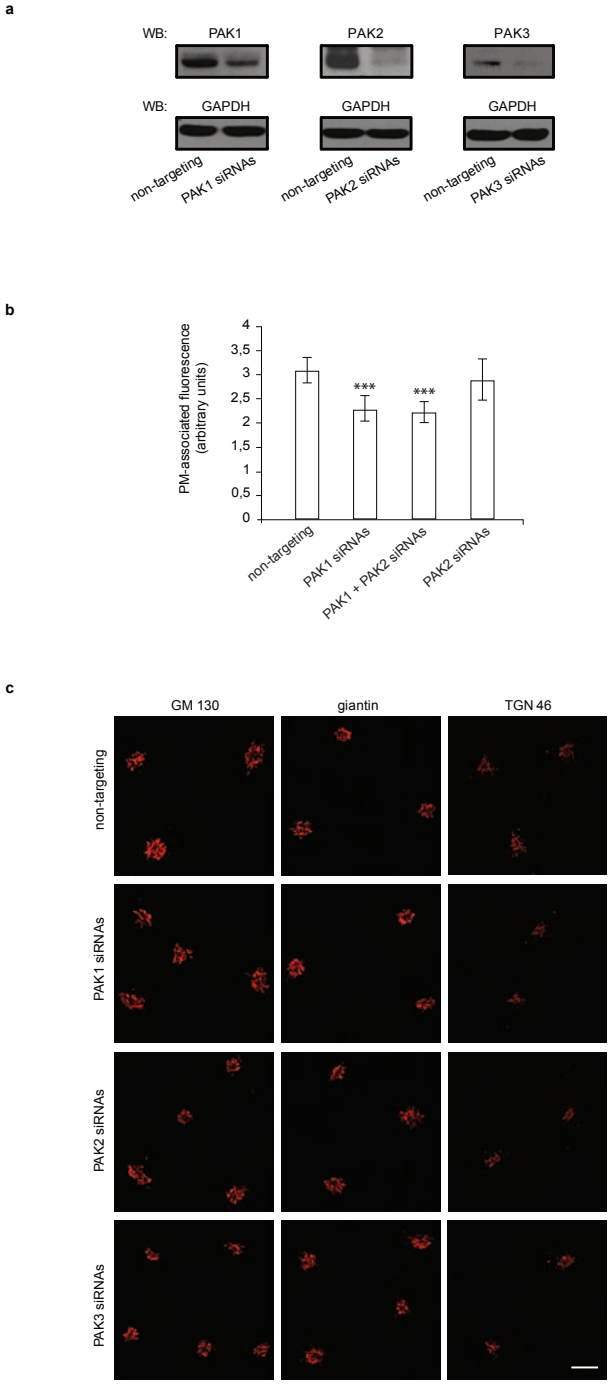


**Figure S8** Effects of PAKs 1-3 on VSVG arrival to the plasma membrane and on the organisation of the Golgi complex. COS7 cells were transfected with non-targeting or PAK1, PAK2, PAK3 or PAK1+PAK2 siRNAs (as indicated) for 48 h. **(a)** Representative blots of cells processed for immunoblotting of PAK1, PAK2 and PAK3 knock-down, as revealed with anti-PAK1, anti-PAK2, anti-PAK3 and anti-GAPDH antibodies. **(b)** The cells were infected with VSV and subjected to the TGN-exit assay. Cell were fixed 60 min after the 32°C temperature-block release. Plasma membrane VSVG was stained without permeabilisation (lumenal domain anti-VSVG antibody). Total VSVG was stained after permeabilisation (P5D4 anti-VSVG antibody). Quantification of plasma membrane-associated VSVG as ratio of plasma membrane:total VSVG. Data are means ±s.d. of three independent experiments. ***P <0.005 (Student's *t*-test). **(c)** Representative images of cells labelled with anti-GM 130, or anti-giantin or anti-TGN 46 antibodies (red), to monitor the structure of the Golgi complex, as indicated. Scale bar, 10 μm.

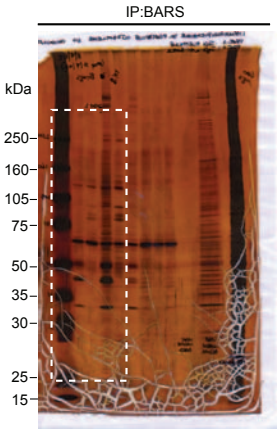


Fig. 1a

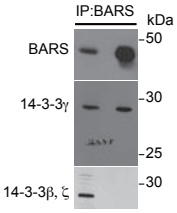


Fig. 1b

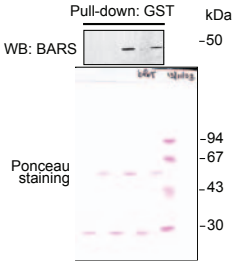


Fig. 1c

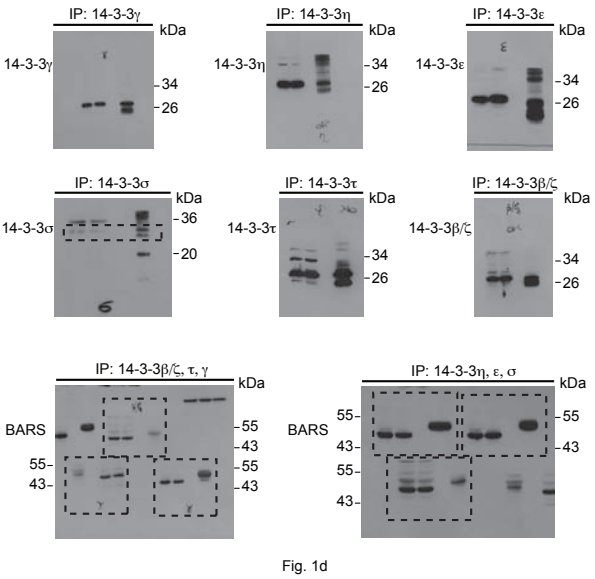


Fig. 1d

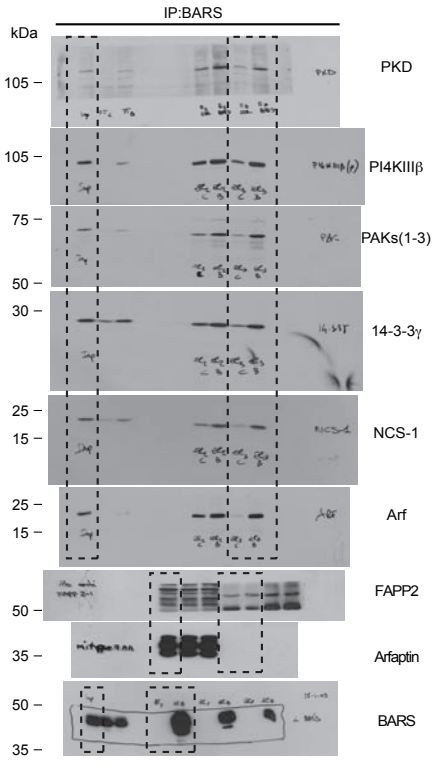


Fig. 1e

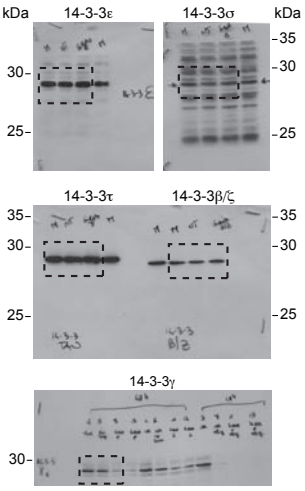


Fig. 2a

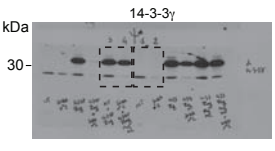


Fig. 2b

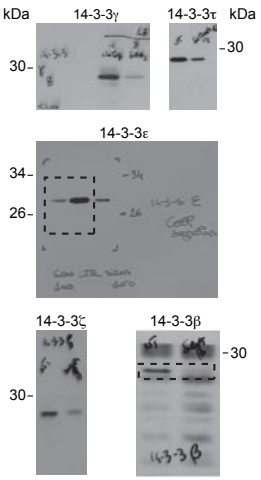


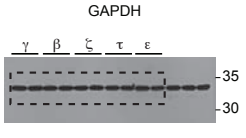


Fig. 3a

**Figure S9** Full scan images of all gel/Western blotting data.

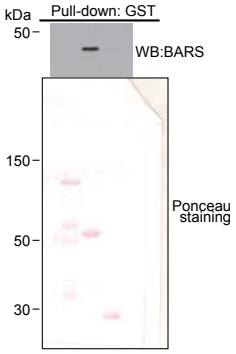


Fig. 4a

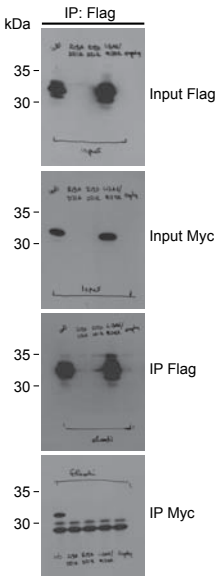


Fig. 4b

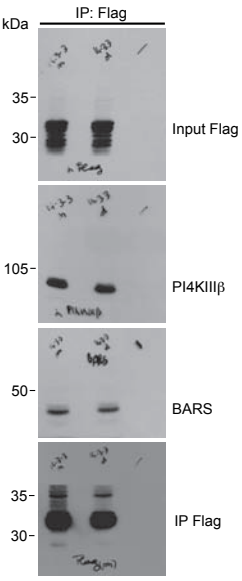


Fig. 4c

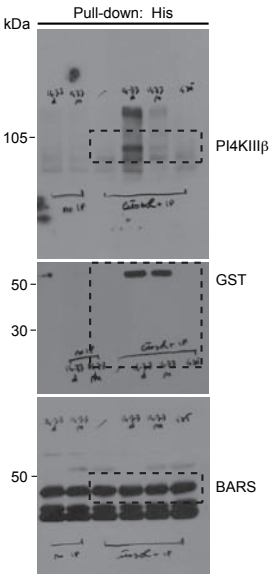


Fig. 4d

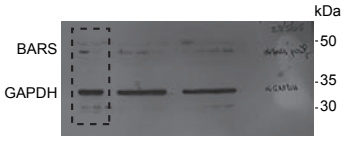


Fig. 6a

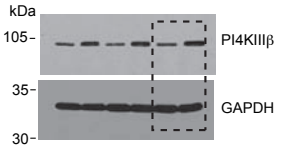


Fig. 6e

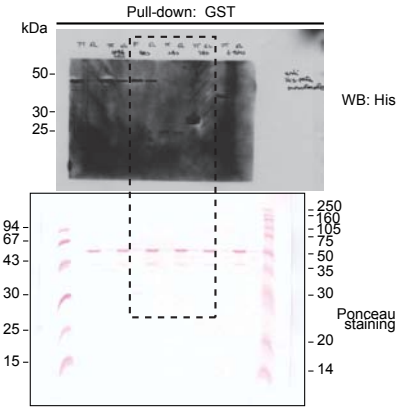


Fig. 7a

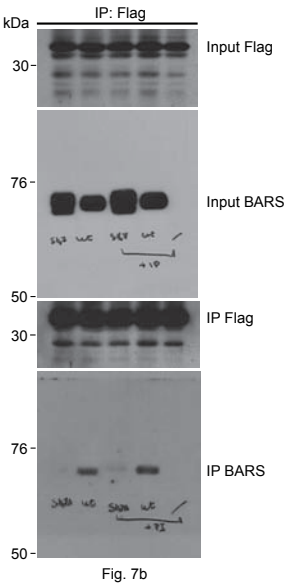


Fig. 7b

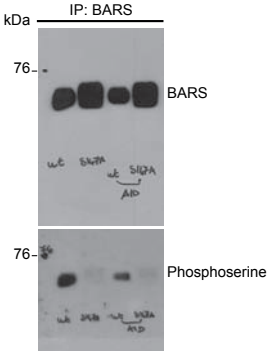


Fig. 7d

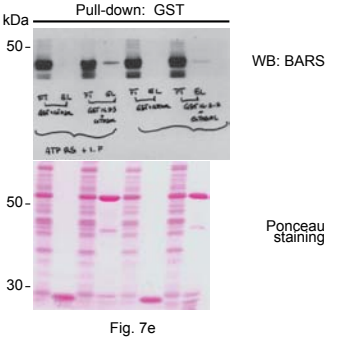


Fig. 7e

**Figure S9 continued**

**Figure S8**

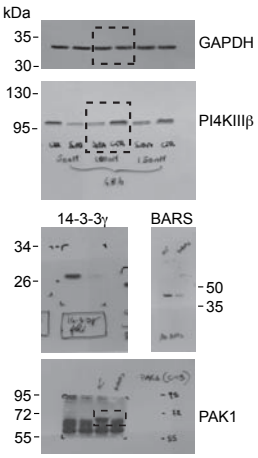


Fig. 8a

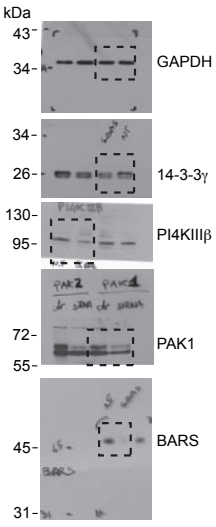


Fig. 8b

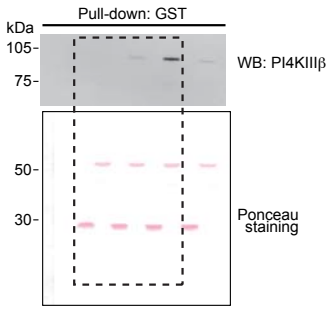


Fig. S2a

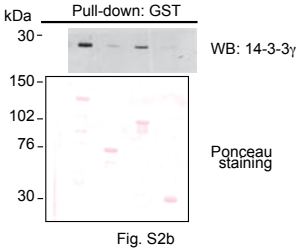


Fig. S2b

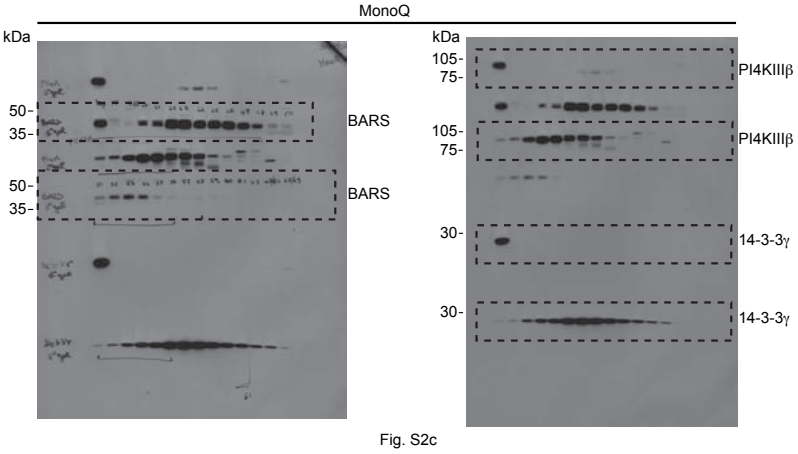


Fig. S2c

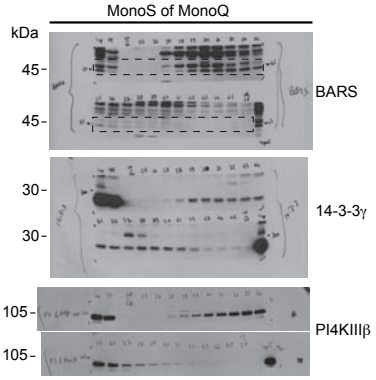


Fig. S2c

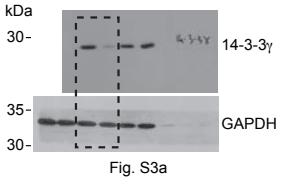


Fig. S3a

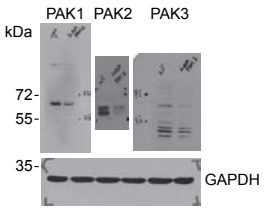


Fig. S8a

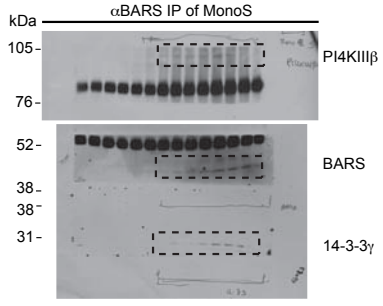


Fig. S2c

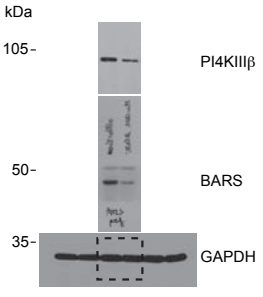


Fig. S4a

**Figure S9 continued**

**Supplementary Tables**

**Table 1** List of the oligonucleotide sequences for amplification of the templates, and of the restriction enzymes used in the cloning of the listed expression vectors.

**Table 2** List of the sequences of the Dharmacon SiRNAs used.

**Supplementary Movies**

**Movie S1** Export of VSVG-GFP from the Golgi complex in COS7 cells following non-targeting siRNAs. Following the non-targeting siRNAs treatment, the cells were transfected for 24 h with VSVG-GFP, subjected to the TGN-exit assay, and observed at 32 °C *in vivo* under confocal microscopy. Insets, right panels are details corresponding to the dashed box regions of the cells. The extrusion, fission, movement and fusion steps of the formed PGC as they move to the PM are indicated by arrowheads. Playback rate: 20 frames $s^{-1}$ with 2 s intervals between frames.

**Movie S2** Export of VSVG-GFP from the Golgi complex in COS7 cells following 14-3-3γ-targeting siRNAs. Following the 14-3-3γ-targeting siRNAs treatment, the cells were transfected for 24 h with VSVG-GFP, subjected to the TGN-exit assay, and observed at 32 °C *in vivo* under confocal microscopy. Insets, right panels are details corresponding to the dashed box regions of the cells. The arrowheads indicate the PGC tubular precursors extending from the Golgi complex and then retracting back into the Golgi complex. Some VSVG-GFP-positive carriers can be seen to still exit from the Golgi complex and to move across the cell towards the PM. Playback rate: 20 frames $s^{-1}$ with 2 s intervals between frames.

**Movie S3** Post-Golgi-carrier formation in COS7 cells expressing BARS-YFP following 14-3-3γ-targeting siRNAs. Following the 14-3-3γ-targeting treatment, the cells were co-transfected with BARS-YFP and VSVG-CFP (for 15 h) and subjected to the TGN-exit assay. PGCs were observed *in vivo* at 32 °C under a Till Photonics imaging system. Left panel: merge; middle panel: VSVG-CFP; right panel: BARS-YFP. Playback rate: 20 frames $s^{-1}$ with 1 s intervals between frames.

**Movie S4** Post-Golgi-carrier formation in COS7 cells expressing BARS-YFP following non-targeting siRNAs. Following the non-targeting siRNAs treatment, the cells were co-transfected with BARS-YFP and VSVG-CFP (for 15 h) and subjected to the TGN-exit assay. PGCs were observed *in vivo* at 32 °C under a Till Photonics imaging system. The arrowhead indicates BARS localisation. Left panel: merge; middle panel: VSVG-CFP; right panel: BARS-YFP. Playback rate: 20 frames $s^{-1}$ with 1 s intervals between frames.

**Movie S5** Formation of post-Golgi-carrier in $BARS^{S147A}$-YFP-expressing cell. COS7 cells were co-transfected with $BARS^{S147A}$-YFP and VSVG-CFP (for 15 h) and subjected to the TGN-exit assay. PGCs were observed *in vivo* at 32 °C under a Till Photonics imaging system. The arrowhead indicates PGC tubular precursor extending from the Golgi complex and not able to undergo fission. Left panel: VSVG-CFP; right panel: BARS-YFP. Playback rate: 20 frames $s^{-1}$ with 1 s intervals between frames.